SMAP RFI Environment Characterization and Residual RFI Mitigation

Undergraduate Research Thesis

Presented in Partial Fulfillment of the Requirements for the Bachelor of Science Graduation with Honors Research Distinction in the College of Engineering of The Ohio State University

by

Matt Daehn
Department of Electrical and Computer Engineering
The Ohio State University
December 2019

Advisor: Dr. Joel Johnson

TABLE OF CONTENTS

ABSTRACT

The Soil Moisture Active/Passive (SMAP) satellite is a NASA mission that aims to provide global soil moisture data. The satellite payload is an L-band microwave radiometer that measures thermal emission from the Earth, and a complex model is used to retrieve soil moisture from the thermal emission data. The SMAP radiometer takes measurements in the frequency band of 1400-1427 MHz, which is supposed to be a protected band for passive remote sensing and therefore to be free of human produced transmissions by international regulations. However, there is clear evidence of radio frequency interference (RFI) in these frequencies due to neighboring transmissions and illegally operating sources. There are a number of RFI detection and mitigation algorithms in place to filter out RFI; however, some residual RFI are still present even after the application of all existing algorithms. This thesis offers an analysis of the RFI environment over time as well as a new technique to estimate the contribution of residual RFI on the filtered data.

ACKNOWLEDGEMENTS

The completion of this research thesis would not have been possible without the assistance of Professor Johnson and weekly meetings with Dr. Alexandra Bringer. I would not have been able to complete this research thesis without their patience, countless hours of their time, and the great opportunity they have given me by allowing me to work with them on this project. In addition to Professor Johnson and Dr. Bringer, I have had many great professional mentors as an undergraduate that have spent significant one on one time with me to build my skills far beyond what I've learned in the classroom while furthering my interest in these types of projects: Dr. Yongbo Wan of Ohio State's Center for Design and Manufacturing Excellence, Dr. Bill Thomas of

NASA Goddard Space Flight Center (GSFC), Paulo Uribe of NASA GSFC, and George Suarez of NASA GSFC. Additionally, I would like to thank the College of Engineering for their financial assistance.

INTRODUCTION

The Soil Moisture Active/Passive (SMAP) satellite launched in January 2015 [1]. It has an onboard radiometer which measures the Earth's thermal emission in the L-band of the microwave spectrum. While the frequencies SMAP measures are protected, SMAP measurements are corrupted by radio frequency interference (RFI) from transmitters operating in the band as well as adjacent bands [2]. In order to mitigate the effects of RFI, nine algorithms were implemented that exploit the properties of Earth's natural emissions. The data is processed into both subband and fullband footprints, and these algorithms operate either on fullband or subband data. The subband data refer to the frequency domain and the subband footprint is a spectrogram using the 16 frequency channels, each with 8 time measurements. The fullband dataset refers to the time domain and a fullband footprint consists of 32 time measurements. Each footprint is taken in either the H or V polarization or 3^{rd} or 4^{th} stokes parameter.

The pulse detection algorithm looks for rapid changes of the brightness temperature in each footprint. The algorithm aims to filter out short duration, high amplitude pulses. It operates on the fullband footprints, and takes an average value after removing the highest 10% of samples in order to remove any bias that might exist due to RFI. Next, all points are compared to the average, and if they differ by more than a multiple of the standard deviation, the point is flagged as RFI. More formally, a measurement is flagged as RFI if:

$$T_A - m \geq \beta_{td}\, \sigma_{td}$$

where T_A is a particular antenna temperature measurement measured in Kelvin, m is the mean, β_{td} is a constant adjusted post launch, and σ_{td} is the standard deviation of the footprint [2].

The cross-frequency detection algorithm exploits the fact that natural emissions increase or decrease gradually over frequency channels. The cross-frequency detection algorithm is similar to the pulse detection algorithm, but it looks for sudden increases across frequency as opposed to time. It best filters out sources that are strong over a narrow range of frequencies. This algorithm operates on subband footprints. For each time, the algorithm looks at all frequency channels and flags any measurements that are a multiple of the standard deviation above the mean. The algorithm will also flag the two adjacent frequency channels of the impacted channel to account for potential leakage into adjacent channels.

The kurtosis detection algorithm exploits the fact that the distribution of natural emissions when sampled should be close to a normal distribution. The kurtosis of each measurement is compared to a nominal value, 3 for a Gaussian distribution, and the measurement is flagged as RFI if the difference is more than a multiple of the standard deviation. That is, a measurement will be as RFI flagged if:

$$|K - K_{nom}| > \beta_k \sigma_k$$

where K_{nom} is a nominal kurtosis value determined prior to launch, β_k is a constant particular to the location, and σ_k is the standard deviation of kurtosis values for the footprint. This algorithm is applied to both the subband and fullband data [2].

The polarization detection algorithm exploits the fact that the polarization of natural emissions is known. This algorithm compares the third and fourth Stokes parameters to a

nominal value, and flags a point as RFI if it is greater than a particular threshold that was defined in post launch analysis of the data. That is, a measurement will be flagged as RFI if:

$$|T_{3,4}| \geq \beta_{3,4}$$

where $T_{3,4}$ is the particular third or fourth Stokes parameter value, $\beta_{3,4}$ is a constant that was set after launch. This algorithm operates on both the subband and fullband data [2].

When RFI is detected, the original measured antenna temperature is replaced with a filtered value. The filtered value is calculated by introducing a Maximum Probability of Detection (MPD) flag, which is the logical OR of the nine algorithms. If a measurement is flagged in a fullband footprint, then all 16 frequency channels for that same time are considered corrupted by RFI as well. The filtered value is then calculated by averaging the remaining pixels of the subband spectrograms that were not flagged by the MPD algorithm. The difference between the measured value and the filtered value is called the RFI level, and is measured in Kelvin [2].

While an overall good performance of these algorithms have been demonstrated [3], some types of RFI have proven to be particularly difficult to flag by the current algorithms. Those undetected RFI are usually continuous wideband RFI. Since it is continuous, it will raise the value of all measurements of a fullband footprint, making the pulse detection algorithm ineffective. Since it is wideband, it will raise the value of all pixels in the subband spectrogram, making the cross-frequency algorithm ineffective as well. Those residual RFI were identified by analyzing a max-hold map of the filtered antenna temperature. An example of this map is presented in Figure 1.

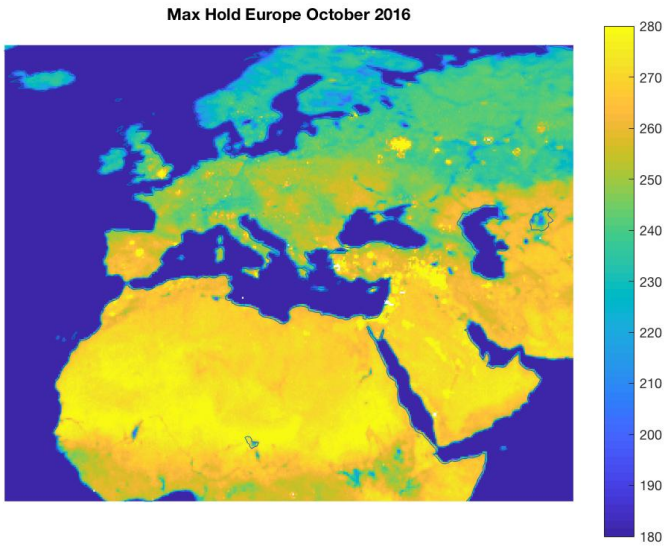

Figure 1: Max Hold Map of Europe Over October 2016

The max-hold map consists in keeping the highest filtered measurement for a considered pixel over a period of time. Figure 1 is the result of max-hold map using a week of data in October 2016. Since most RFI typically skew a measurement higher, this map will show residual RFI to appear "hotter" than the surrounding areas, for instance, the bright yellow spots in Figure 1 are places identified as locations with residual RFI.

This thesis will examine the changes in the RFI environment over time, and provide analysis of data output by a tool developed in collaboration between the Ohio State University and NASA Goddard Space Flight Center. This tool weekly produces a table containing the most persistent and strongest RFI sources. These tables have been produced since the beginning of the mission, and their analysis can provide useful information on the change of the RFI environment over the 3+ years of the mission. This information could prove valuable for the development of future missions, as well as for the reporting of offending sources to authorities.

Additionally, this thesis proposes to investigate a new method to further filter some of the residual RFI present in Figure 1. Unlike the algorithms that currently look at one footprint at a time, this method is based on a time series analysis. The method exploits the fact that in a RFI free area, the measured antenna temperature is expected to vary following the seasonal pattern of the physical temperature. However, in locations identified as having residual RFI, these seasonal variations can be obscured or corrupted by RFI. By looking at nearby locations without residual RFI and using Fourier transforms, estimates of the true antenna temperatures can be reconstructed. The success of this method would ultimately improve the soil moisture retrievals that SMAP produces.

METHODOLOGY

I. RFI Environment Characterization

A tool was developed in collaboration between the Ohio State University and NASA Goddard Space Flight Center (GSFC) to output a list of RFI sources weekly. The list is the merged result of two lists: one produced by The Ohio State University which provides statistical information about the RFI sources, and one produced by GSFC which provides precise locations and RFI levels of the sources. To be listed in the table, a source must meet two criteria: it must have an RFI level higher than 10 K, and be visible in more than 25% of SMAP overpasses in the previous month [4]. This selects sources that are both high in amplitude and persistent. The tables have been generated weekly since April 2015, allowing for long term analysis of the most active and high RFI level sources.

The tables provide information about the RFI environment and can be used to track its changes with time. The analysis can also be performed first, globally, and then in more details with the analysis of individual continents. The first and most obvious change tracked globally was the number of sources that appeared in the tables over time and is presented in Figure 2.

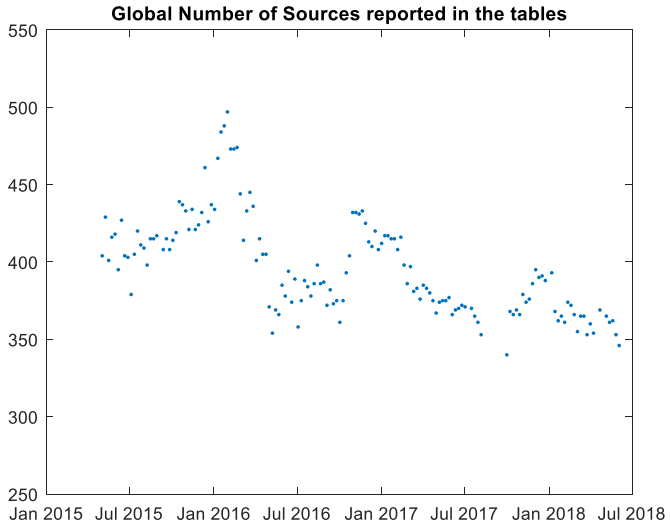

Figure 2: Number of RFI Sources Reported Globally Over Time

Since the mission began, it appears that the number of sources that meet the criteria to be listed in the tables slightly decreases with time indicating a potential improvement in the RFI environment as fewer strong sources are currently observed than at the beginning of the mission. In addition, the number of sources seems to follow a seasonal pattern, increasing in the winter and decreasing in the summer.

The number of sources over time can further be broken down into continents. This analysis is presented Figure 3. The continent analysis allows for identification of which parts of the world are responsible for the variations observed in the overall trend as well as the global concentration of RFI sources.

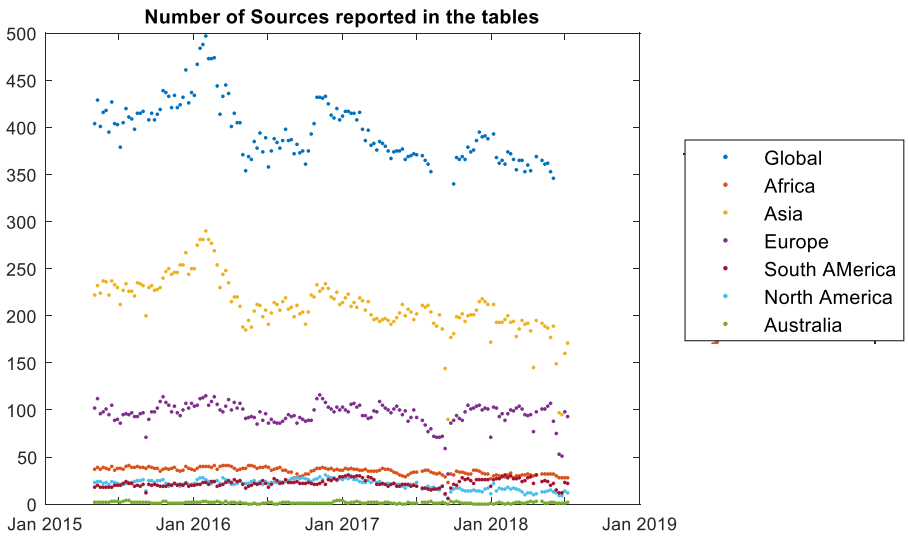

Figure 3: Number of Sources By Country Over Time

Indeed, Figure 3 reveals that the seasonal pattern as well as the overall decrease in number of sources over time is primarily due to Asia. The other continents have a relatively stable number of sources over time. Additionally, it reveals that Asia has the largest number of sources, followed by Europe and Africa.

In addition to plotting the number of sources globally over time, an analysis of the averages of the statistics over time can also be performed. The tables track maximum RFI level, mean RFI level, time percentage, and the MPD flagging percentage, which is a measure of the number of measurements flagged by the algorithms as containing RFI divided by the total number of measurements.

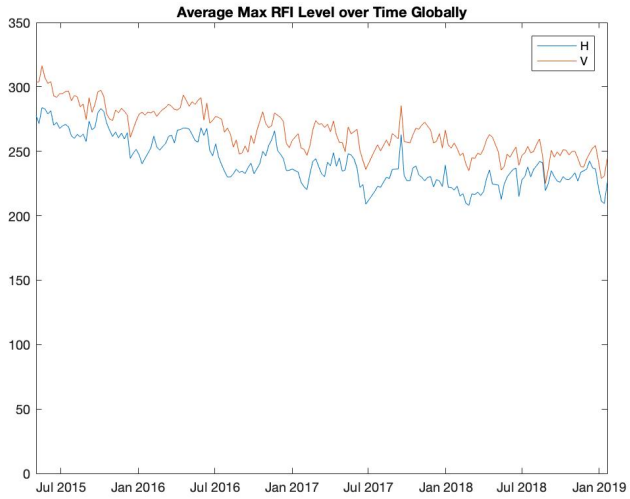

Figure 4: Global Average Maximum RFI Level

Figure 4 shows that the global average maximum RFI level has decreased by about 50 K over the life of the mission. Global averages of the remaining statistics present in the table over the life of the mission can be found in the Appendix. These plots taken together show that while the statistics of individual sources may vary significantly over time, the global averages of these statistics have remained fairly steady over time.

The tables allow for the averages of these statistics to be taken at the continent, country, and regional level in addition to globally. The Appendix includes plots of the average of the statistics present in the table for each continent over the life of the mission. These averages allow a rough trend to be deduced over time, and by taking them at various scales, it becomes possible to pinpoint which smaller regions are driving the changes in the larger overall pattern. Detailed analyses of the changes in the RFI environment over time were performed using this approach for two continents: Africa and Europe.

For the analysis of Africa, the starting point was the average Maximum RFI Level reported in the tables. Figure 5 shows this average taken across Africa over the life of the SMAP mission. Figure 5 shows the average maximum RFI level rising nearly 100 K around January 2018 and remaining steadily higher after this date.

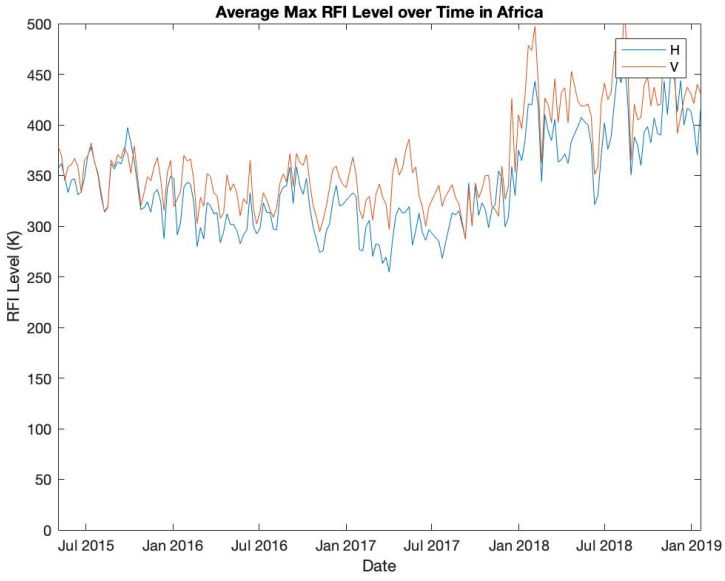

Figure 5: Average Max RFI over Time In Africa

In order to determine the cause of this increase, Africa was divided up into six regions: Northwest Region 1 consisted of Morocco, Western Sahara, Mauritania, Algeria, Tunisia, Mali, Senegal, Gambia, and Guinea Bissau; Northwest Region 2 consisted of Guinea, Sierra Leone, Liberia, Cote d'Ivoire, Ghana, Burkina Faso, Togo, Benin, Nigeria, Niger, and Cameroon; Northeast Region 1 consisted of Libya and Egypt; Northeast Region 2 consisted of Sudan, Chad, Eritrea, Djibouti, South Sudan, Ethiopia, and the Central African Republic; The Southeast Region consisted of Uganda, Kenya, Rwanda, Burundi, Tanzania, Malawi, Zambia, Mozambique, Zimbabwe, Swaziland, and Madagascar; The Southwest Region consisted of Equatorial Guinea, Gabon,

Republic of the Congo, Democratic Republic of the Congo, Angola, Namibia, Botswana, South Africa, and Lesotho. Figure 6 shows the definition of the regions.

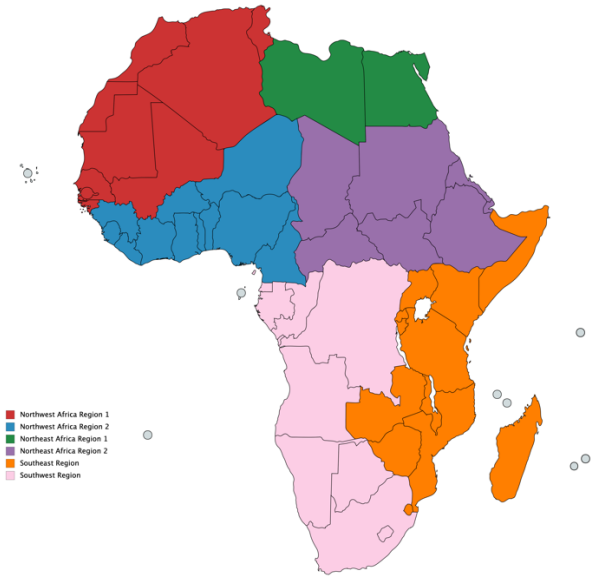

Figure 6: Regions of Africa

Plots were generated that tracked the average statistics in each region over time, in addition to the number of sources each region had present in the tables over the life of the mission. These plots revealed that the cause of the increase in average Maximum RFI level around January 2018 present in Figure 5 was likely the Southeast Region, highlighted in orange in Figure 6. Figure 7 shows the average Max RFI Level over this region, which also spikes around January 2018 and remains consistently higher after this time.

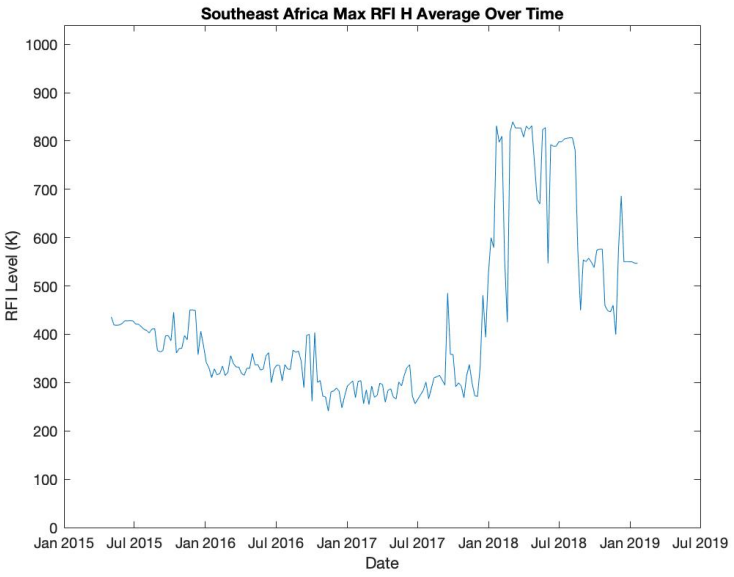

Figure 7: Average Max RFI Level H Over Southeast Africa

In addition to the average Maximum RFI Level increasing suddenly around January 2018, the number of sources in this region visible in the tables also decreased suddenly. Figure 8 shows this trend.

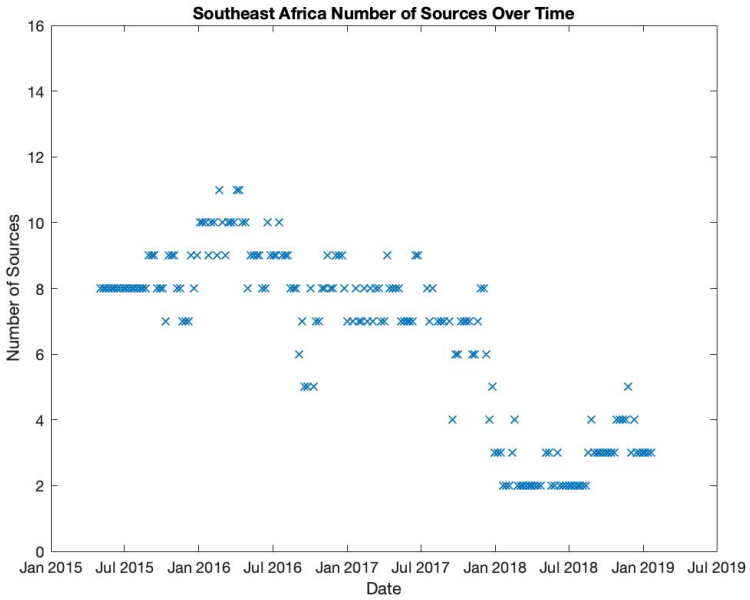

Figure 8: Number of Persistent RFI in Southeast Africa

Figure 9 shows the Maximum RFI Level over the life of the mission for each source in this region. It appears that around January 2018, a number of low amplitude RFI sources stopped emitting, while higher amplitude sources continued to emit. The reduction of low amplitude sources raised the average over the region. This increase in average over the region actually indicates an improvement in the RFI situation in this region, contrary to initial expectations.

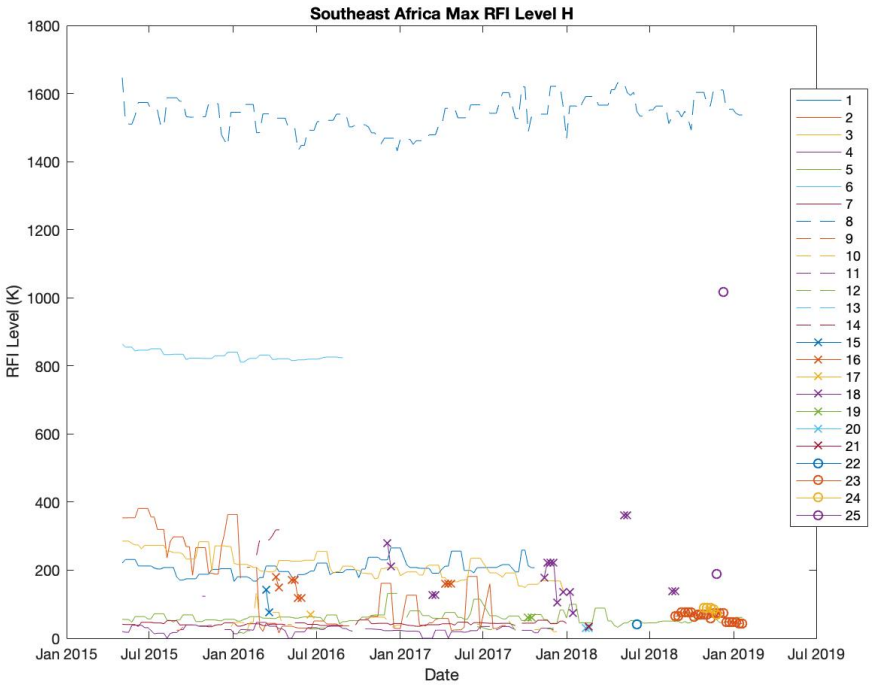

Figure 9: Southeast Africa Max RFI Level H For All Sources

In the same way Africa was broken up into regions, Europe was broken into 27 regions due to a large number of RFI sources. Overall, the RFI environment in Europe appears to be quite stable.

In addition to averages, histograms of the statistics over time can be produced based on information in the tables. The Appendix contains histograms over the life of the mission for the statistics in the tables taken globally, and at the continent level. The histograms do not contain

information on variation over time, but provide information on the distribution of entries in the tables. The global histograms show the typical properties of RFI sources in the L-band. Globally, about 55% of table entries have a maximum RFI level in the H polarization less than 300 K, while about 70% of table entries have a maximum RFI level less than 300 K in the V polarization. In the H polarization, only about 5% of table entries have a maximum RFI level above 1400 K. In the V polarization, only about 5% of table entries have a maximum RFI level above 1000 K. The distribution for mean RFI level is much more condensed, with 83% of table entries having mean RFI levels less than 200 K in the H polarization, and 75% having mean RFI levels less than 200 K in the V polarization. The distributions of MPD flagging percentage are right-skewed, with the most common value somewhere between 35 and 40%. Very few table entries have MPD flagging percentages below 10% or above 90%. The global histograms also reveal that approximately half of table have time percentages between 95 and 100%. Very few have time percentages below 20%, which should be expected as the tables select for persistent sources.

The histograms at the continent level reveal how the properties of RFI sources vary regionally. The histograms show that Africa has a higher proportion than the global average of sites with a high MPD flagging percentage. Australia has no sites with a maximum RFI level above around 700 K, and has more high amplitude sites in the H polarization than the V polarization. Additionally, the Time Percentage statistics for Australia are quite different than any other continent, with no strong preference for sites active nearly 100% of the time. North America also has a higher proportion of sources than typical with Time Percentages in the 30-80% range. Asia, Europe, and South America all match the global proportions fairly closely.

In addition to using the tables to perform analysis on large quantities of sources, individual sources can be tracked by using the latitude and longitude listed in the table. When tracking individual sources from week to week, the exact latitude and longitude listed in the tables can vary slightly. This makes it necessary to have a working definition for what can be treated as one source over multiple weeks. GSFC developed an algorithm to precisely locate RFI sources. Therefore, they provide a set of lat-lon coordinates for each source as well as an uncertainty that depends on the number of overpasses and the RFI strength.

For the purposes of this thesis, table entries will be considered as part of the same source if they are within the uncertainty of another entry, or they are "connected" through other entries that are within each other's uncertainties. For example, two entries do not need to be within each other's uncertainties to be considered the same source if there is a third entry in between that shares uncertainties with each of the two entries. Figure 10 illustrates this concept, with the red X's placed at the latitudes and longitudes listed in the tables, and the black circles as the uncertainties around that location. While the X's at the highest and lowest latitudes of the source do not have intersecting uncertainties, there is an unbroken path from each lat-lon pair to any other through the uncertainties in the measurements.

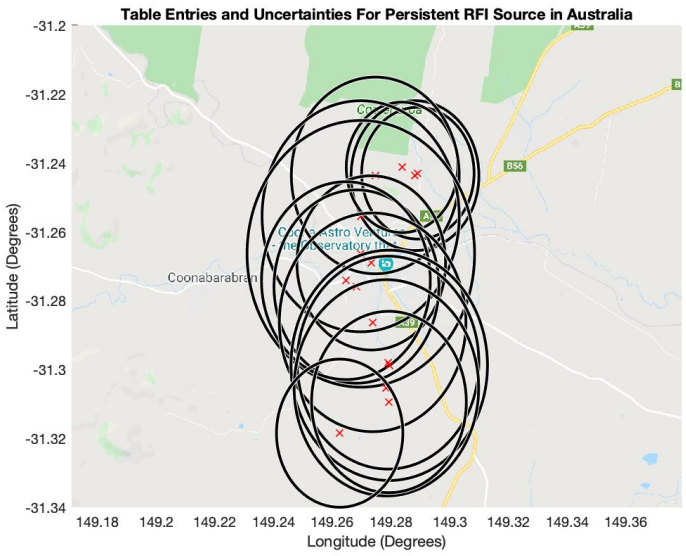

Figure 10: Source Grouping Example

Using this working definition, maps can be created that show the locations of all of the sources listed in the tables. Figure 11 shows a map of all of the sources that appeared in the tables from the beginning of the mission until the end of January 2019.

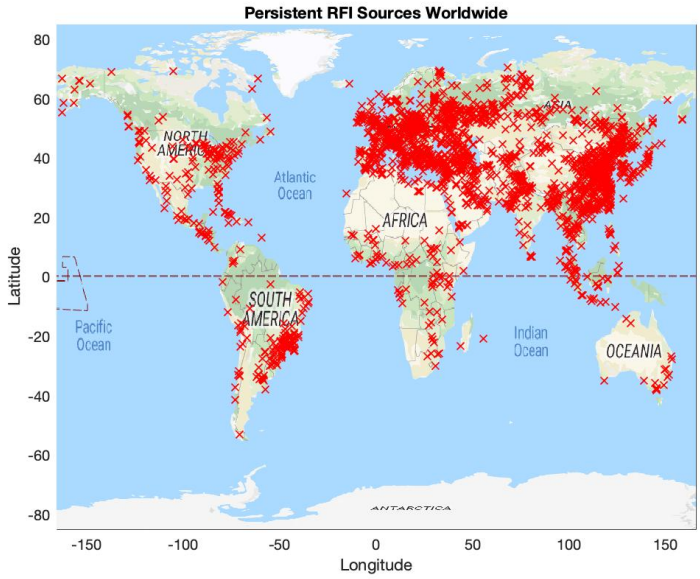

Figure 11: The Persistent RFI Sources Worldwide

This map shows that Europe, Asia, and the Middle East have the highest concentration of persistent, high amplitude RFI sources, and Figures 12 and 13 show zoomed in views of these heavily affected regions.

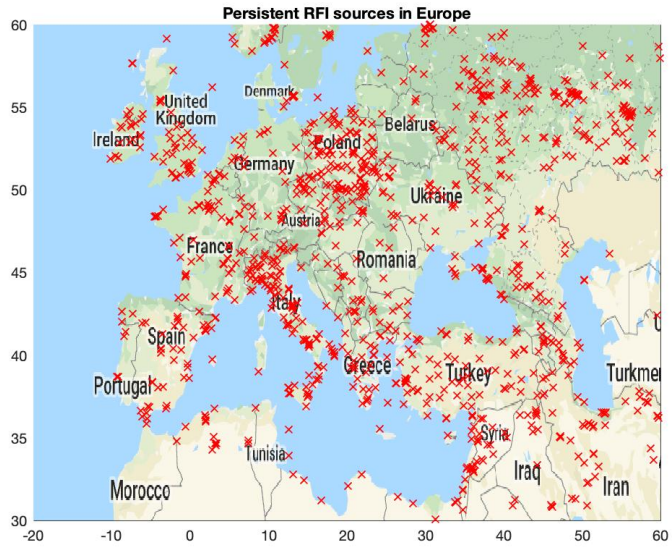

Figure 12: Persistent RFI Sources of Europe

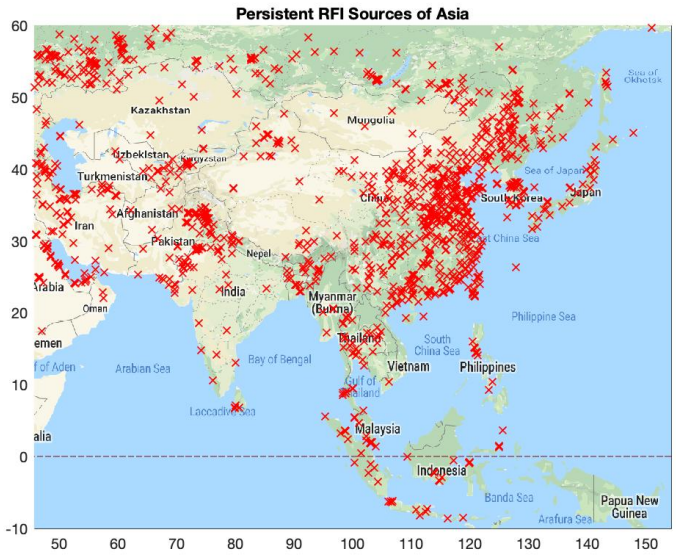

Figure 13: Persistent RFI Sources of Asia

In addition to revealing a distribution of RFI sources, the tables can be utilized to look at the statistical variations of each source over time. In an effort to understand the seasonal pattern

present in Figures 2 and 3, the sources present over Asia were analyzed in order to find sources exhibiting a seasonal pattern. A source was marked as exhibiting seasonal variation if it always showed up in the tables in January and was always absent in June, and continued this pattern for more than one year. 159 such sources were found in the tables. One example of such a source was near Miyazaki, Japan. Figure 14 is a plot of the mean RFI level over time for this source. Time periods with no data present are periods for which the source no longer met the criteria to be listed in the tables, meaning either the persistence or the RFI level of the source dropped.

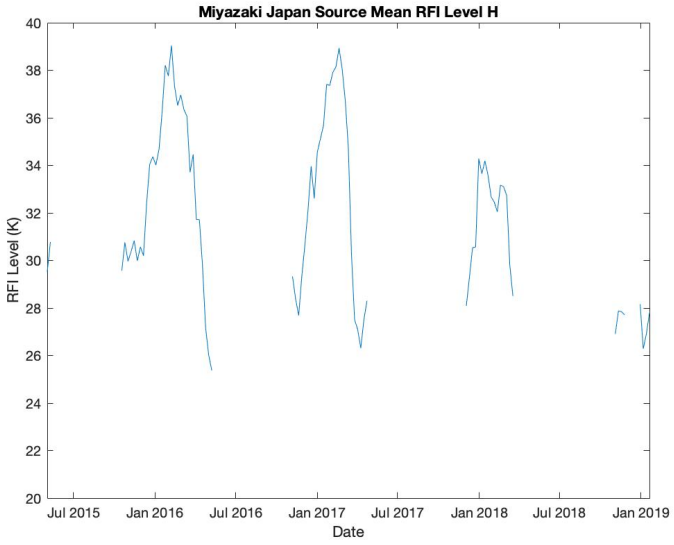

Figure 14: Mean RFI Level of RFI Source Near Miyazaki, Japan

In addition to the RFI level of the source, the frequency channels impacted by RFI can also be analyzed. Figure 15 shows the percentage of time each frequency channel has been found to be impacted by RFI.

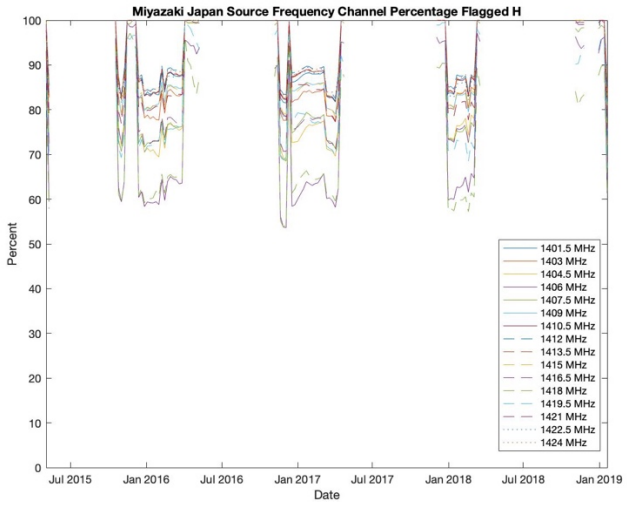

Figure 15: Frequency Flagging of RFI Source Near Miyazaki, Japan

The figure shows that while some frequency channels are more impacted than others, all the frequency channels that SMAP operates over are heavily impacted by RFI over the winter months. Finally, the geographic distribution over which this source was found in the tables is shown in Figure 16.

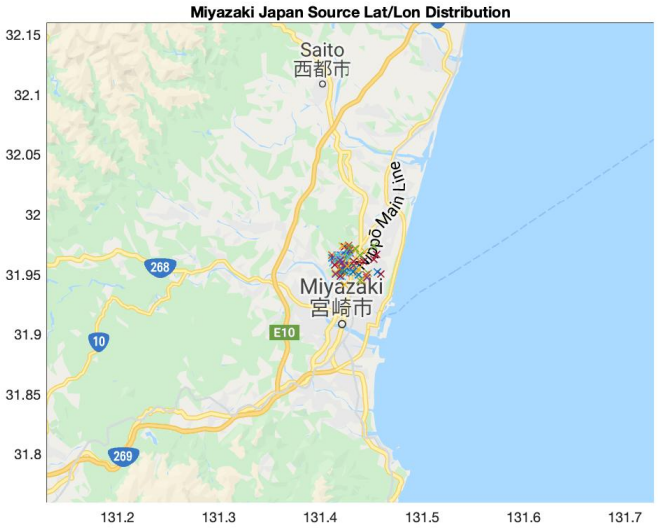

Figure 16: Measured Lat/Lon of Source Near Miyazaki, Japan

Since the tables have been produced for the entire mission, the locations of the strongest and most persistent sources are known for the three years. Therefore, it is possible to investigate the probable cause of those RFI sources. It was found that from the inspection of the coordinates listed in the tables, many of the sources appear to be located close to airports. A more detailed analysis was performed in order to determine the correspondence between RFI emitting sources and airport locations.

Because each source is a collection of table entries, the average latitude and longitude of a source was taken. Each table entry has an associated uncertainty, and the worst case uncertainty for a source was found by taking the table entry farthest from the average location of the source, and adding its uncertainty to the distance that entry is from the source's average latitude and longitude. This gives the largest uncertainty for a particular source. Figure 17 shows the result of this process applied to the RFI source in Figure 10. The red X is the average latitude and longitude coordinates of the site, and the black circle is the worst case uncertainty.

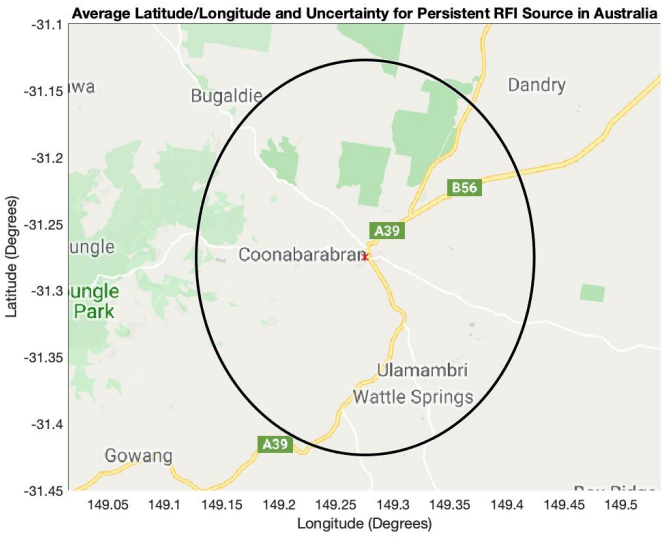

Figure 17: Average Latitude/Longitude and Worst Case Uncertainty for Persistent RFI Source in Australia

Next, a global list of airports was cross-referenced with this list of sources. The sources were grouped by continent, and the percentage of RFI sources in the tables that contained an airport within their uncertainty was calculated. In Africa, 47% of sources are located in the vicinity of an airport; In Asia, 40%; In Australia 95%; In Europe 63%; In North America 91%, In South America 63%. This shows that airport locations are significantly correlated with RFI sources, and they may likely be a significant contributor to the RFI environment.

II. Time Series Analysis to Estimate Residual RFI Contributions

Another part of my work focused on the analysis of time series of SMAP data. Indeed, all of the current RFI detection algorithms operate on footprints, and therefore operate on short timescales. However, these algorithms have proved ineffective at filtering out certain types of RFI such as continuous moderate RFI [5]. As shown in the introduction, these residual sources can be spotted by creating a "Max Hold" map over a longer time period. However, no algorithms or methodology currently exist that leverage time series variations to identify and filter residual RFI.

In an RFI-free area, the antenna temperature is expected to vary seasonally following the seasonal variations of the physical temperature, with regions farther from the equator experiencing greater seasonal variations. Figure 18 shows demonstrates this seasonal pattern. The plotted values are a max hold of the filtered antenna temperature over one week.

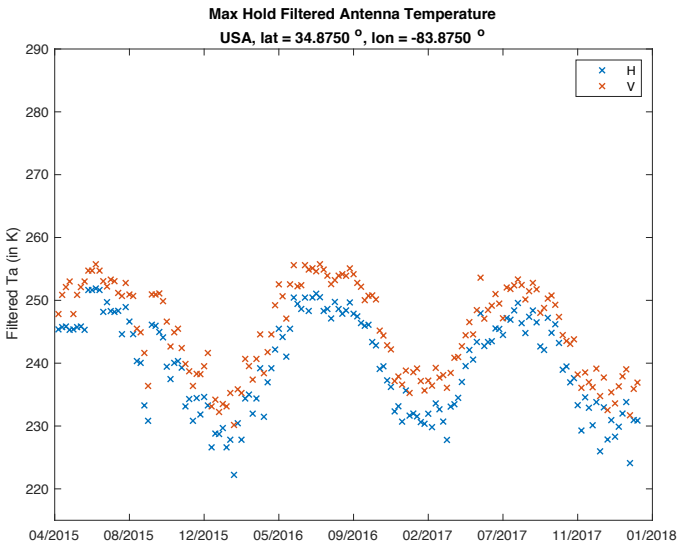

Figure 18: Seasonal Variation of Antenna Temperature in RFI Free Environment [6]

If an area was corrupted by residual RFI, this pattern could be distorted in two significant ways: the average value could be skewed higher while preserving the seasonal pattern, or the pattern itself could be distorted. A persistent residual RFI source will systematically skew the average, while an intermittent source, such as the source near Miyazaki Japan discussed in Part I, will distort the pattern. For this reason, two different methodologies were developed.

In order to distinguish the RFI sources, the persistence can be analyzed. It is defined as the percentage of SMAP overpasses a location has an RFI level greater than 10 K divided by the total number of overpasses. A location with a constant persistence will be processed differently than an area that has a persistence that fluctuates significantly over time. Figure 19 is an example of a source near Beijing, China that has a persistence that varies seasonally, while Figure 20 shows a source near Madrid, Spain that has a relatively constant persistence.

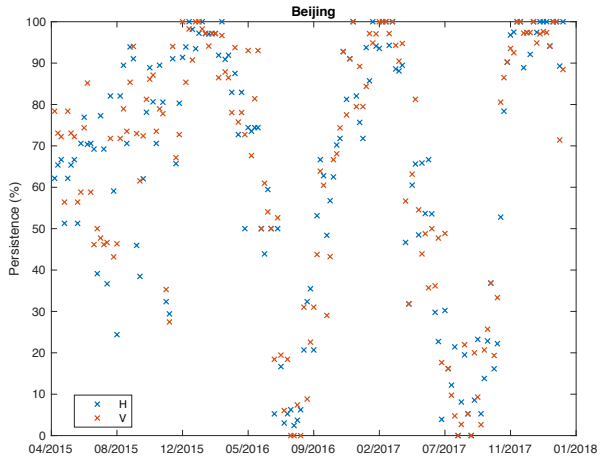

Figure 19: Seasonally Varying Persistence [6]

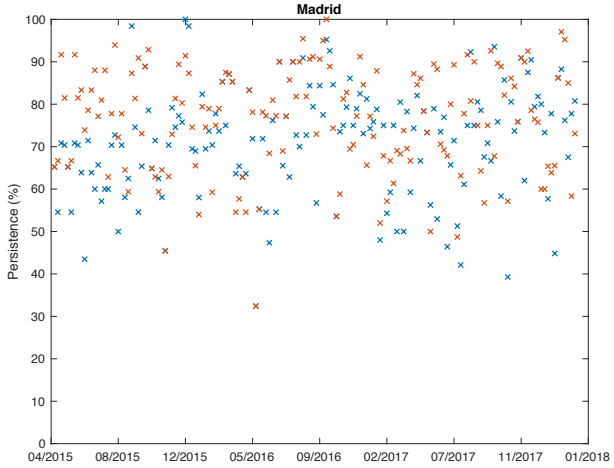

Figure 20: Constant Persistence [6]

While the metric of persistence is based on the existing algorithms, closer analysis reveals that it can also contain information about the likelihood that a location suffers from residual RFI. Indeed, residual RFI locations seem to correspond to areas with high persistence, as illustrated in Figure 21. Figure 21 presents the Max-hold filtered antenna temperature for a source located near Beijing, China. In that case, the highest filtered antenna temperatures are observed when the persistence is maximum. This means that the higher values of the antenna temperature are

more likely to contain residual RFI. This example indicates that persistence can be used as a metric for identifying residual RFI. Moreover, the variations of the persistence with time can also be use to distinguish between the two cases described above.

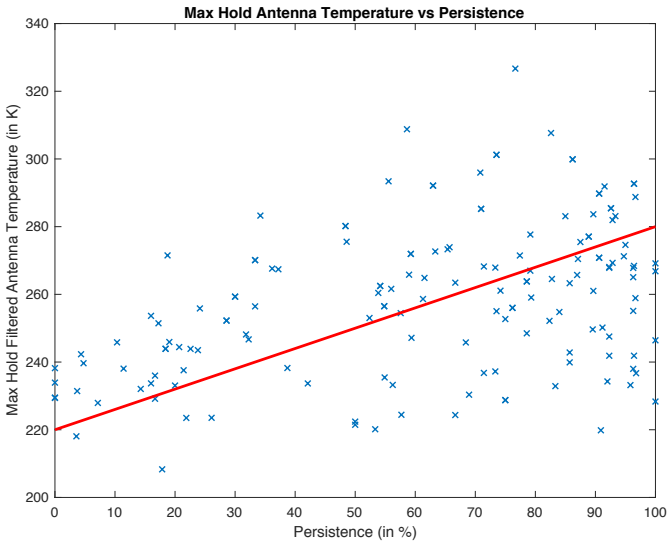

Figure 21: Persistence vs Filtered Antenna Temperature [6]

In the case where the persistence varies significantly over time, the average value of the antenna temperature should be close to the true value, but the seasonal pattern is no longer intact. To remedy this, a Fast Fourier Transform (FFT) can be applied to the max hold of the filtered antenna temperature time series. An example of the max-hold of the filtered antenna temperature time series and its FFT can be seen in Figure 22 and Figure 23, respectively. This example illustrates the RFI source observed in Beijing, China.

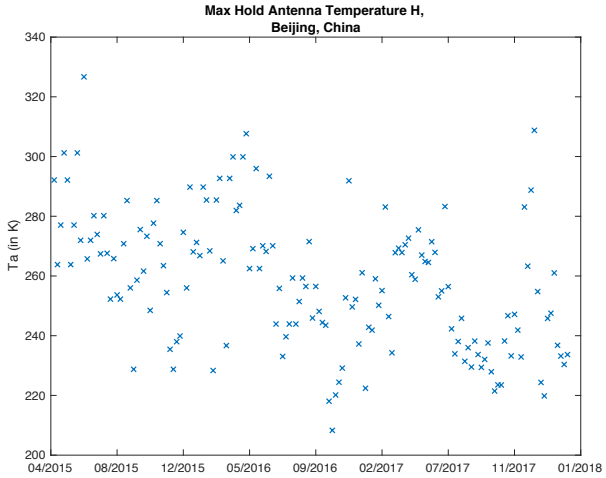

Figure 22: Beijing Filtered Antenna Temperatures [6]

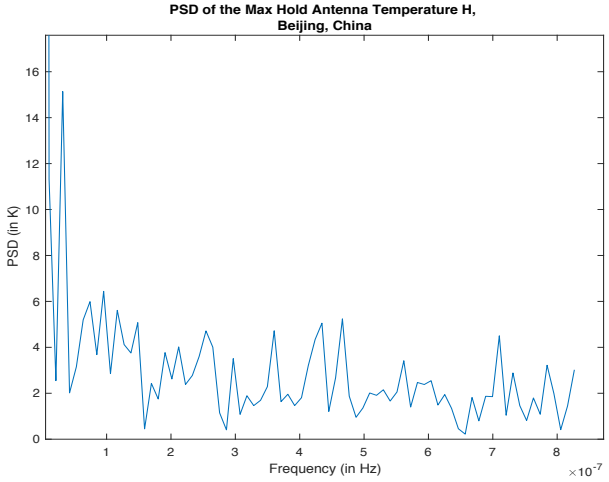

Figure 23: FFT of Antenna Temperatures in Beijing [6]

Although the seasonal pattern is difficult to observe in Figure 22, the frequency corresponding to a period of one year is prominent in the FFT in Figure 23. The remaining significant frequencies are a result of noise and can be discarded. Then, the Inverse Fast Fourier Transform (IFFT) can be applied to reconstruct the expected seasonal pattern.

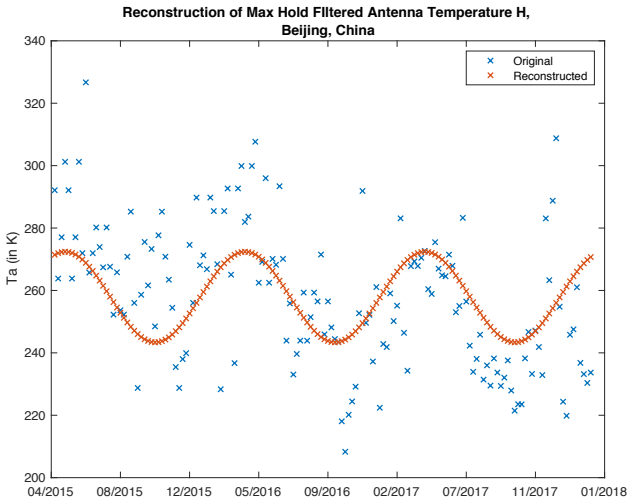

Figure 24: Reconstructed Seasonal Pattern of Beijing Site [6]

Since RFI will typically skew an antenna temperature higher than the natural value, any antenna temperature higher than the reconstruction can be flagged as impacted by RFI, and the residual RFI can be calculated by subtracting the reconstruction from the original value. Figure 25 shows the residual RFI level at this site, which frequently is as high as 40 K.

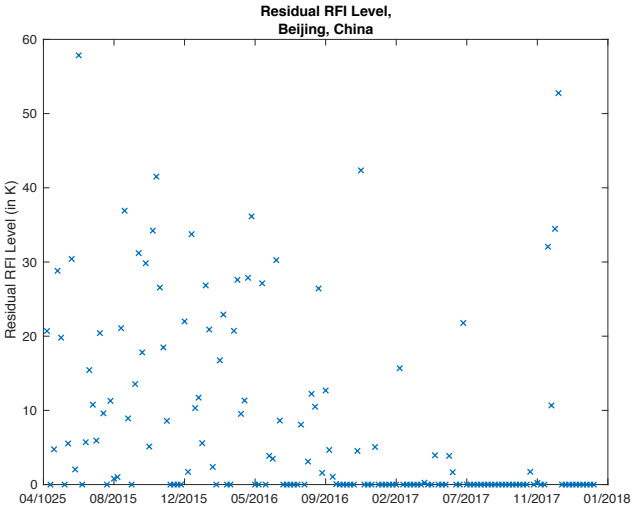

Figure 25: Residual RFI Level at Beijing Site [6]

In the case where the persistence of the RFI level does not present a seasonal variation, the seasonal pattern of the max-hold of the filtered antenna temperature may remain, but will be biased to higher antenna temperature levels. In this case, another methodology is developed based on a spatial algorithm. This method relies on the assumption that nearby locations will naturally have similar thermal emissions.

The method begins by identifying an area of affected pixels from the persistence map for a given week. Then for each pixel of the area identified, a window around the pixel is expanded outwards until at least 25% of the pixels in the window have a persistence close to 0%. Then, each pixel in the window is given a weight equal to one minus the persistence, and the weighted average of the max-hold filtered antenna temperature is calculated. This average replaces the original antenna temperature of that pixel for that week. This process is repeated until less than 20% of the pixels in the impacted area have an antenna temperature of greater than 300 K. An example of the results of this algorithm is presented in Figure 26. Indeed, the reconstructed time series of antenna temperatures for the Madrid Site can be seen in Figure 26 in red and is compared to the original max-hold filtered antenna temperature in blue.

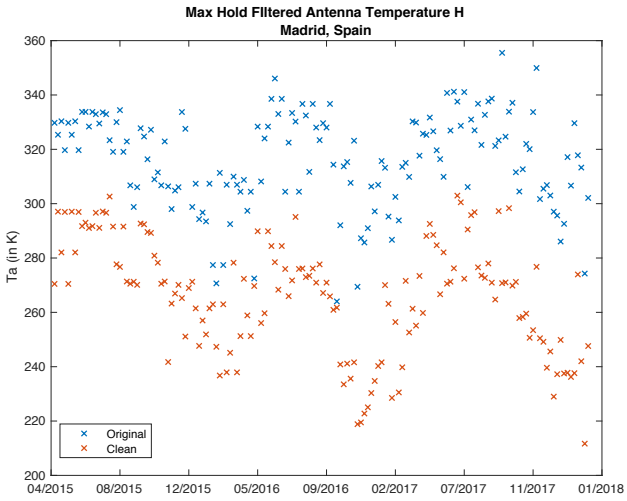

Figure 26: Original and Filtered Antenna Temperatures at Madrid Site [6]

This method preserves the seasonal variation, and a residual RFI level can be calculated by subtracting the "clean" values from the original values. The result for the Madrid site can be seen in Figure 27.

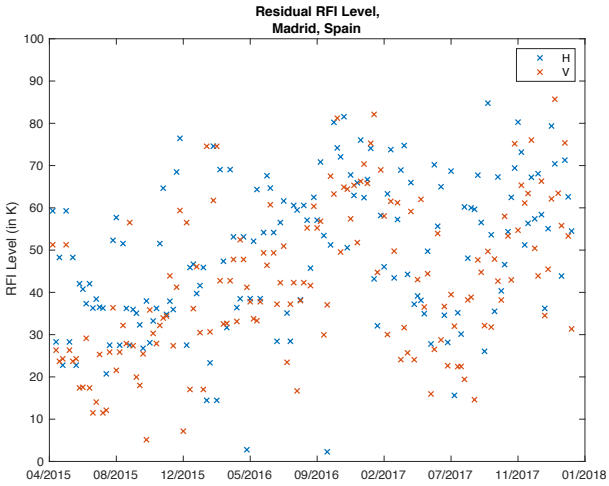

Figure 27: Residual RFI Level at Madrid Site [6]

An automatic tool was developed to identify residual RFI sources and process them with the methods described in this thesis. The tool processed any source that was observed to have

a persistence of more than 25%. Then, the average residual RFI level was calculated globally over the entire mission. Figure 28 displays these results in the H polarization.

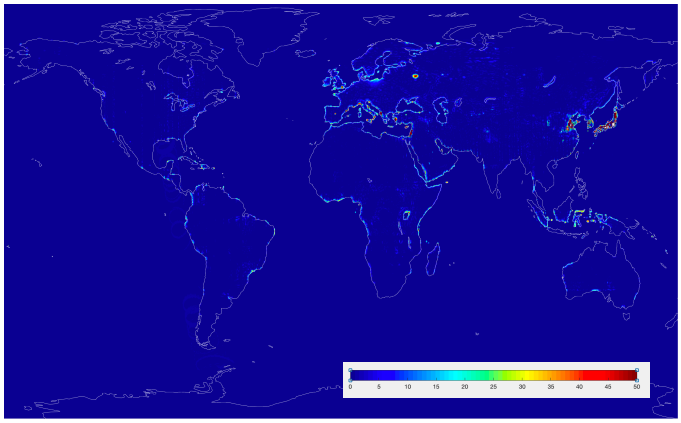

Figure 28: Global Average Residual RFI Level H

The results are encouraging because the automatic tool detects and estimates the contributions of residual RFI in regions known to contain it. However, it also shows that there are areas for future work. The spatial algorithm for persistent sources does not work when there are multiple sources in a small area. This explains why the residual RFI level is so low throughout most of Europe, where there is known to be issues with residual RFI. Additionally, some coastlines are shown to have high residual RFI values. The spatial algorithm currently does not factor in coastlines, so the ocean data used in the average will artificially increase the calculated residual RFI level. Adding an ocean mask will correct this issue. Finally, the parameters of the spatial algorithm may need to be optimized for the best possible performance.

CONCLUSION

The work presented in this thesis summaries two main studies that I performed during my research activities: an analysis of the RFI environment since the SMAP mission began, and a proposed methodology to filter out residual RFI that is currently not well mitigated by existing algorithms.

The RFI environment analysis revealed that Europe, the Middle East, and Asia had the largest amounts of RFI. It was also observed that a large number of Asian sources operate seasonally and that airports are likely a significant RFI contributor. Finally, the RFI environment analysis established the typical properties of the persistent and high amplitude RFI sources in the range of 1400-1427 MHz.

In order to filter residual RFI and estimate its contributions, it is recommended that residual RFI be broken up into two main groups: seasonal sources and persistent sources. Seasonal sources can be mitigated by taking an FFT of the antenna temperature over time, and removing unnatural frequencies. Then, measurements higher than this ideal estimation can be flagged as residual RFI. Persistent sources can be mitigated through an iterative process averaging the antenna temperature of an area that has persistent RFI with the surrounding RFI free regions.

The work presented in this thesis has been presented at two international conferences, and aims to improve the quality and accuracy of measurements taken by SMAP and future remote sensing missions.

APPENDIX

Global Averages of Statistics Found in RFI Tables

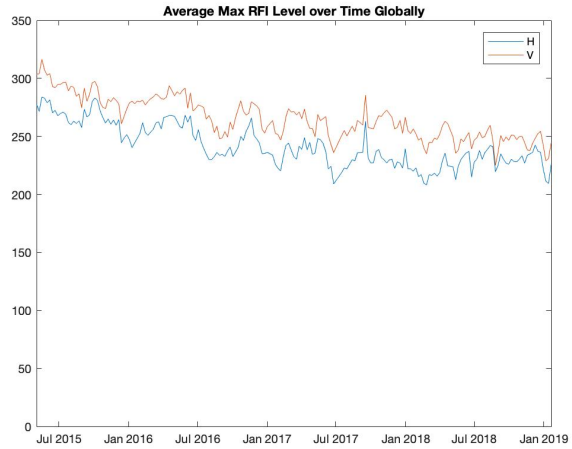

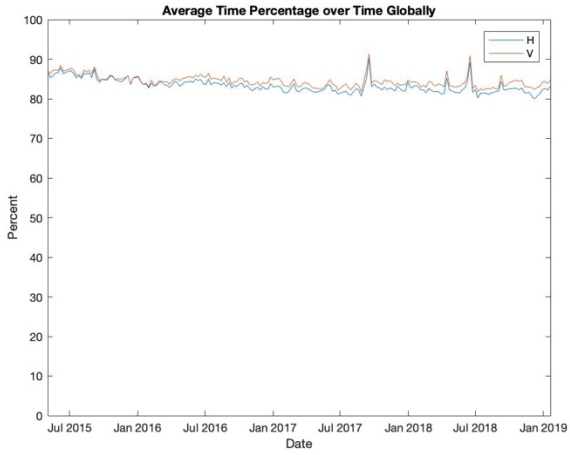

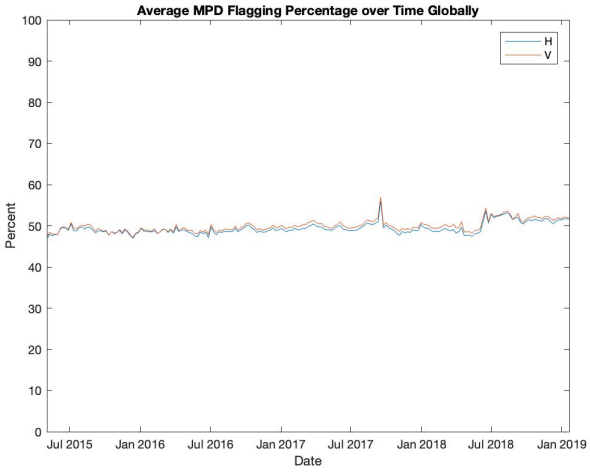

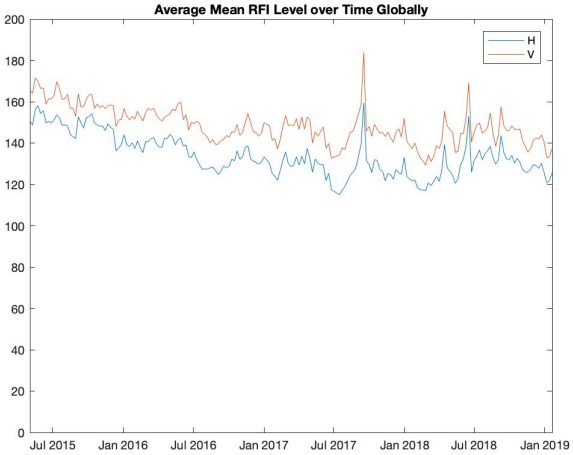

Continental Averages For Statistics in RFI Tables:
Africa

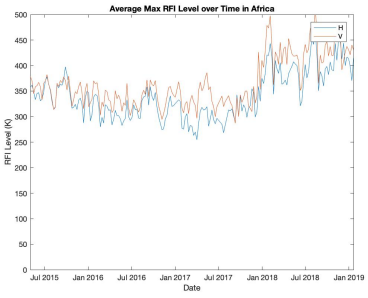

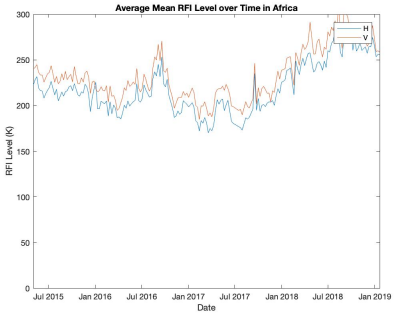

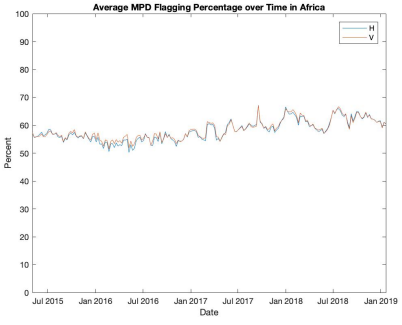

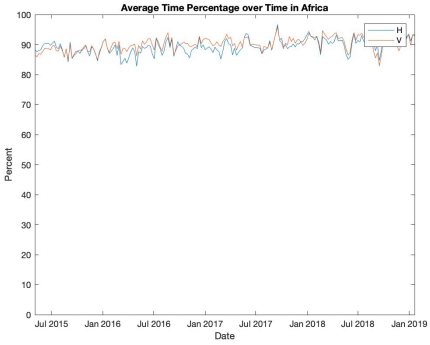

Asia:

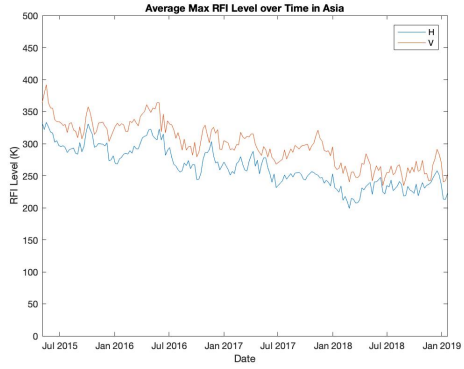

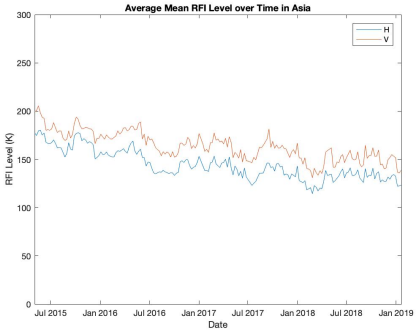

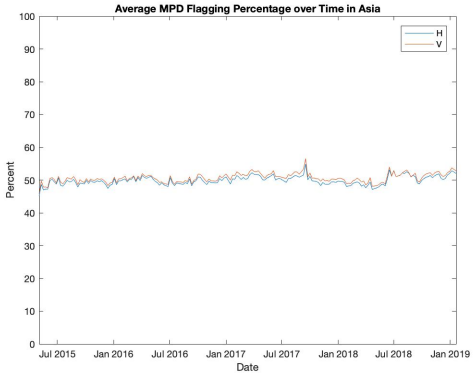

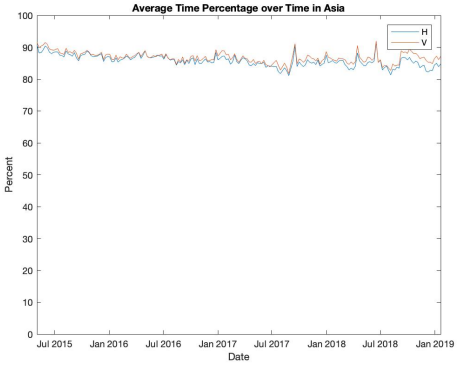

Australia:

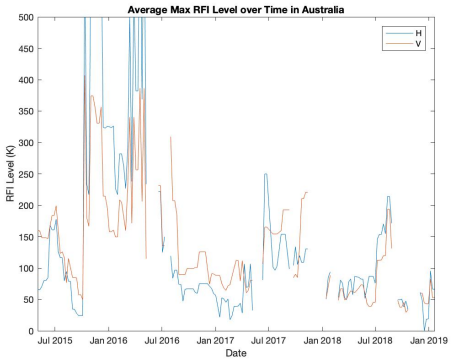

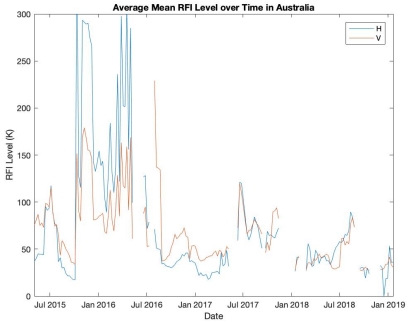

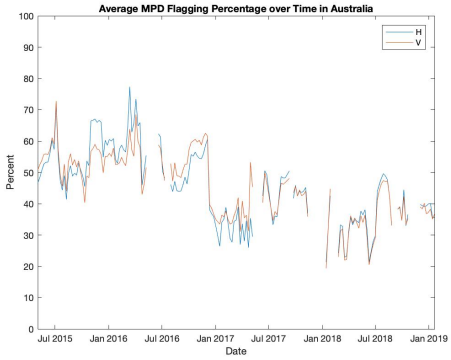

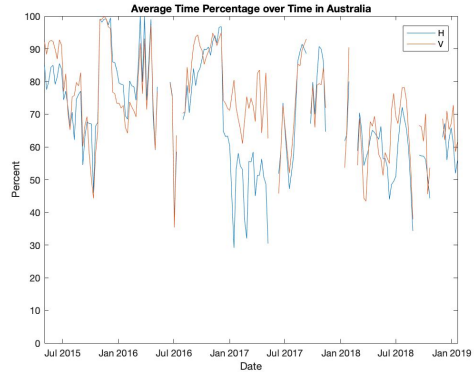

Europe:

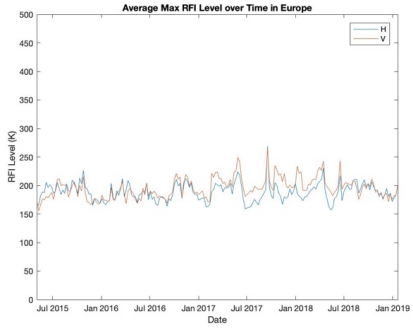

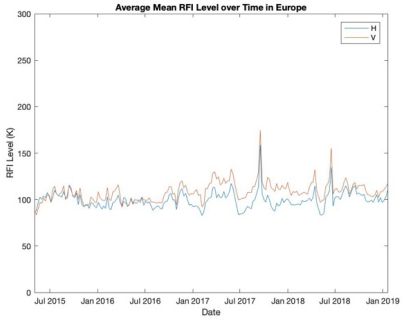

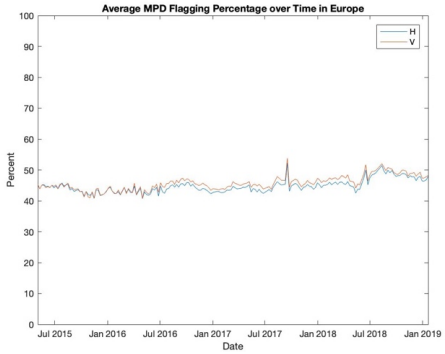

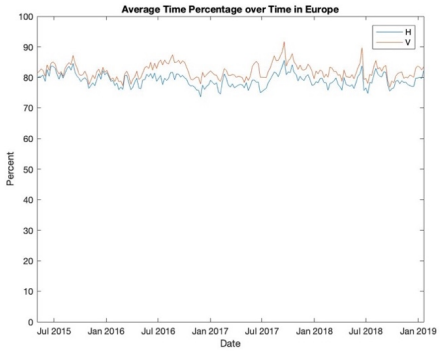

North America:

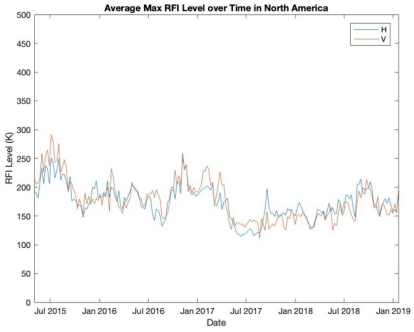

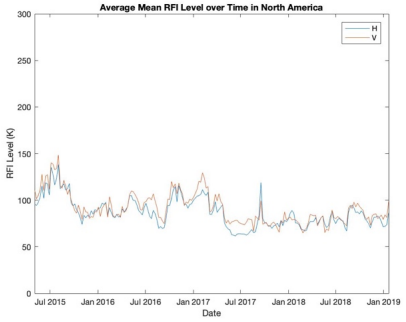

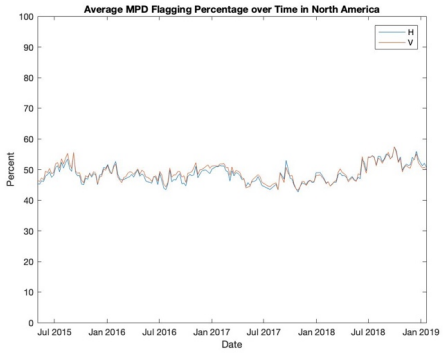

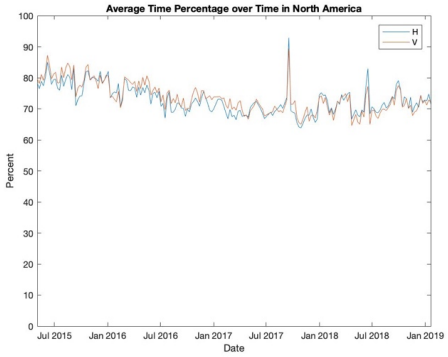

South America:

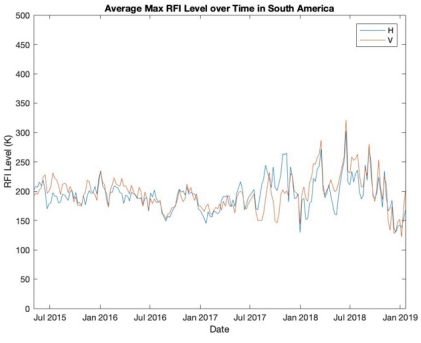

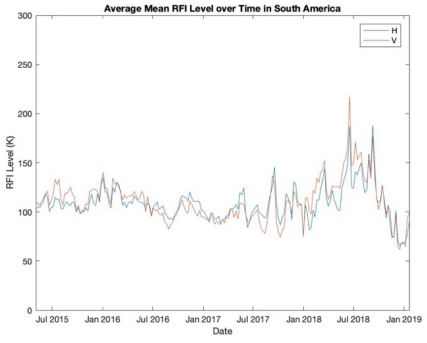

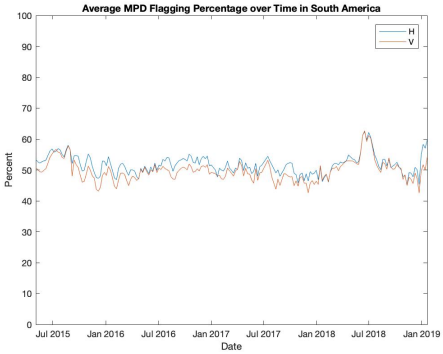

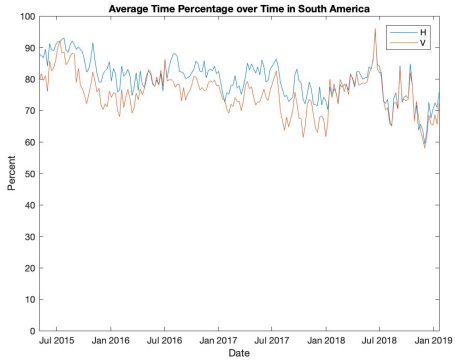

Histograms of Statistics in RFI Tables:

Global:

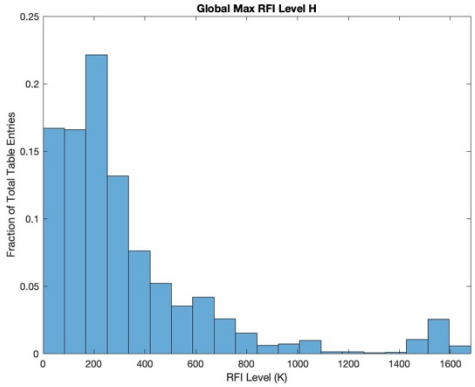

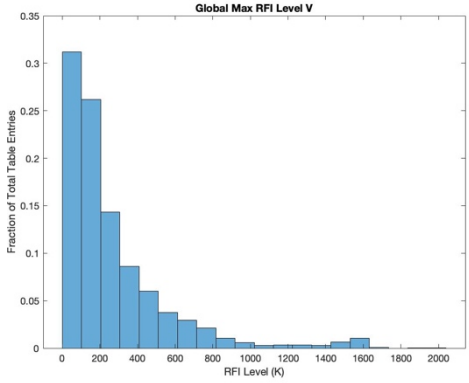

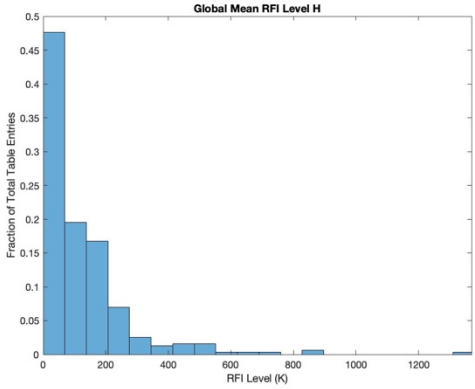

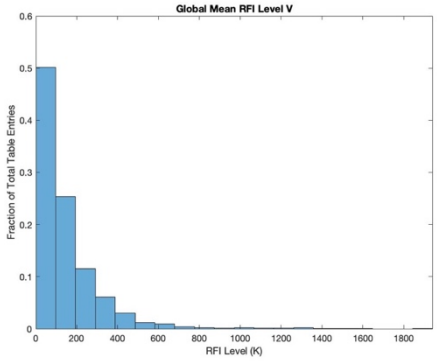

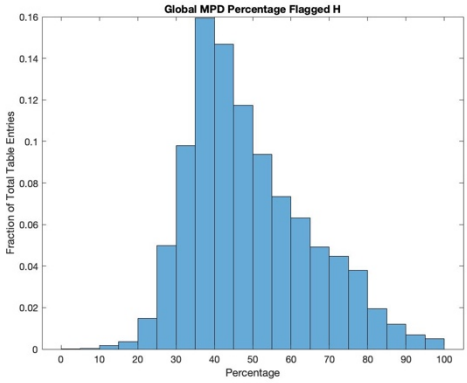

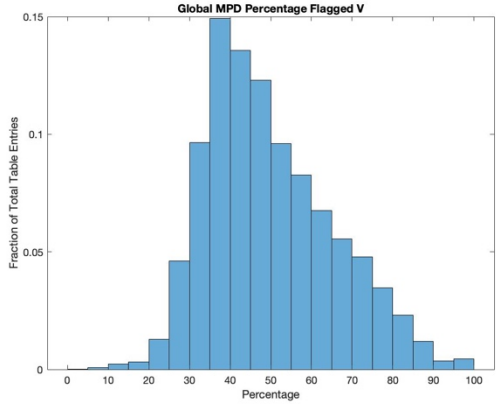

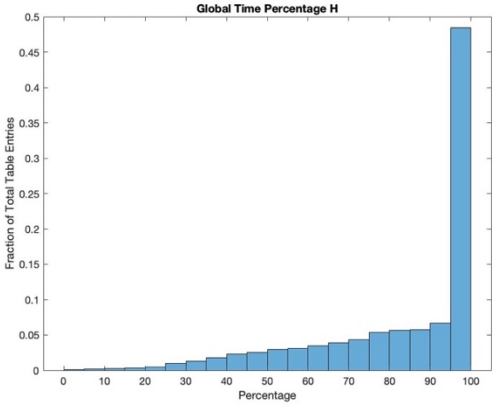

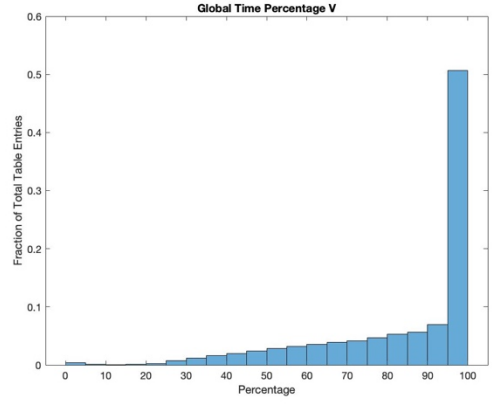

Africa:

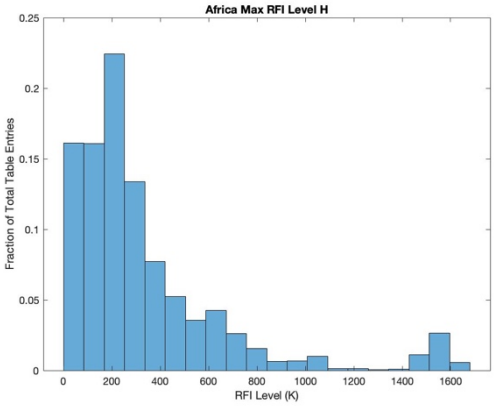
Africa Max RFI Level H
Fraction of Total Table Entries
RFI Level (K)

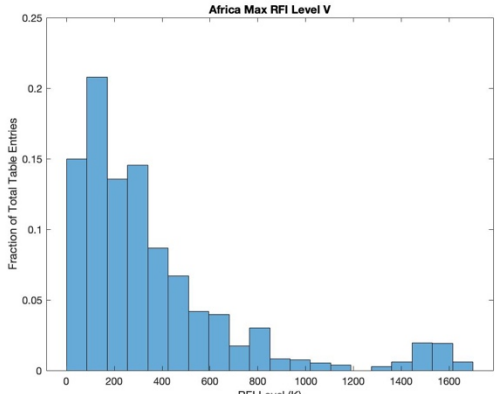
Africa Max RFI Level V
Fraction of Total Table Entries

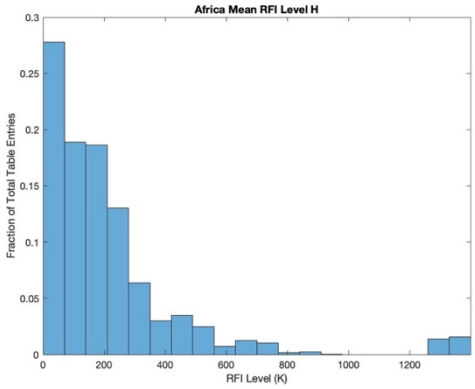
Africa Mean RFI Level H
Fraction of Total Table Entries
RFI Level (K)

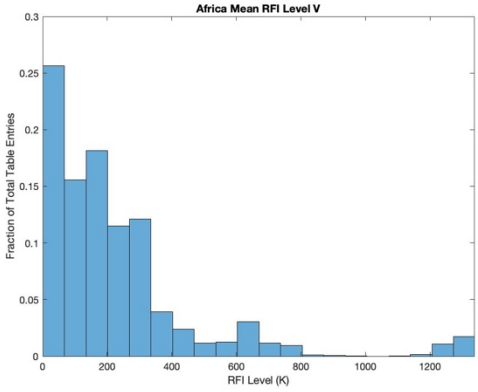
Africa Mean RFI Level V
Fraction of Total Table Entries
RFI Level (K)

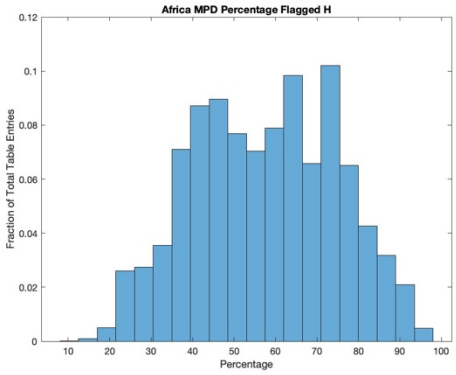
Africa MPD Percentage Flagged H
Fraction of Total Table Entries
Percentage

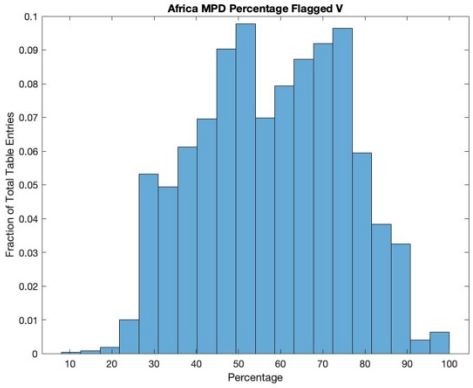
Africa MPD Percentage Flagged V
Fraction of Total Table Entries
Percentage

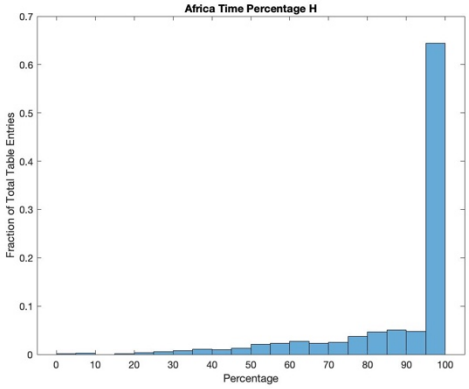
Africa Time Percentage H
Fraction of Total Table Entries
Percentage

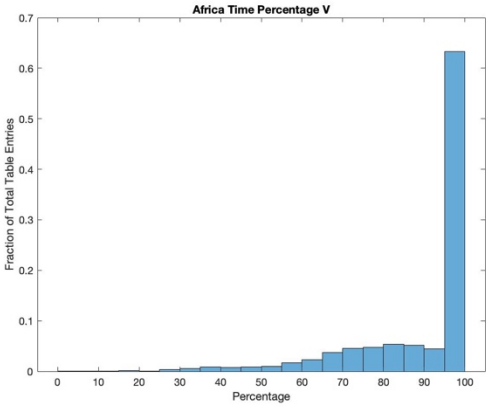
Africa Time Percentage V
Fraction of Total Table Entries
Percentage

Asia:

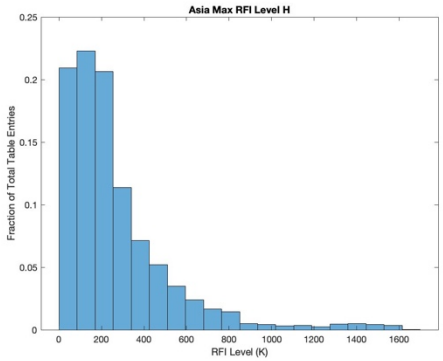
Asia Max RFI Level H
Fraction of Total Table Entries
RFI Level (K)

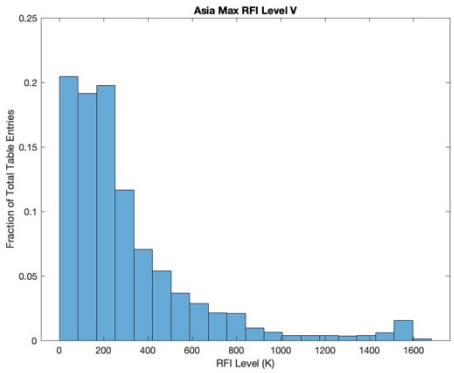
Asia Max RFI Level V
Fraction of Total Table Entries
RFI Level (K)

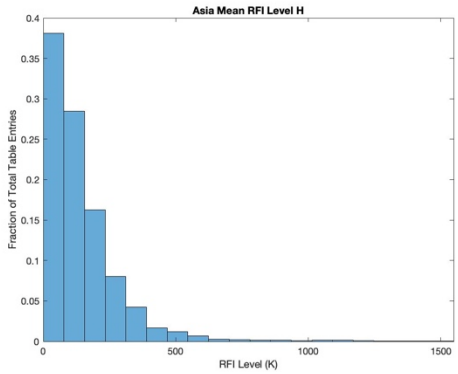
Asia Mean RFI Level H
Fraction of Total Table Entries
RFI Level (K)

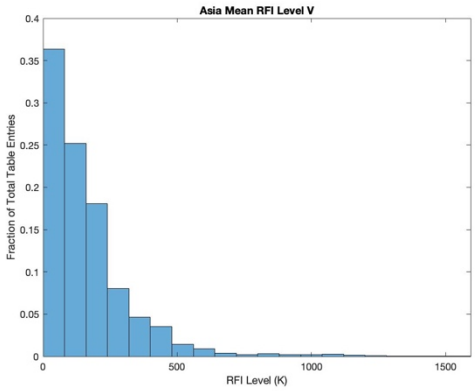
Asia Mean RFI Level V
Fraction of Total Table Entries
RFI Level (K)

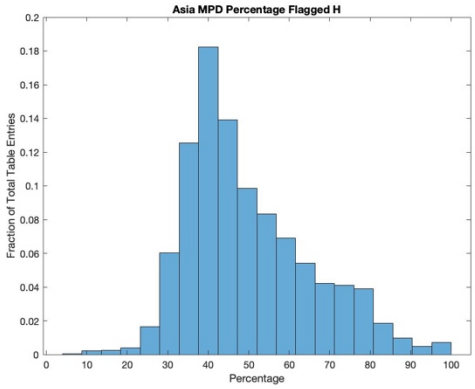
Asia MPD Percentage Flagged H
Fraction of Total Table Entries
Percentage

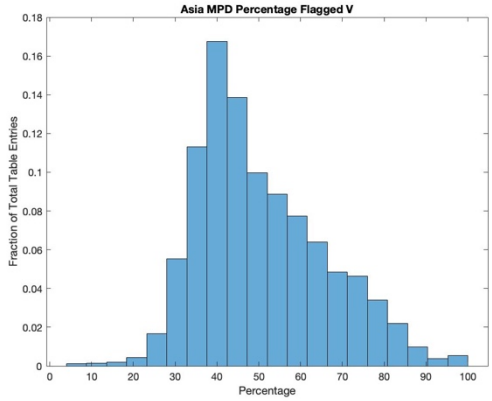
Asia MPD Percentage Flagged V
Fraction of Total Table Entries
Percentage

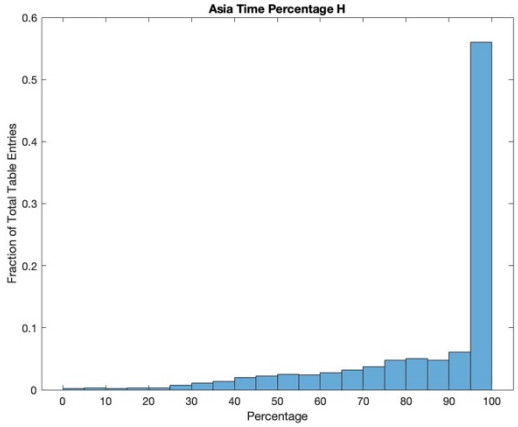
Asia Time Percentage H
Fraction of Total Table Entries
Percentage

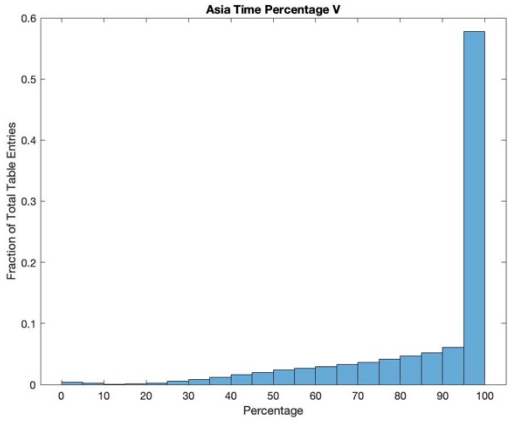
Asia Time Percentage V
Fraction of Total Table Entries
Percentage

Australia:

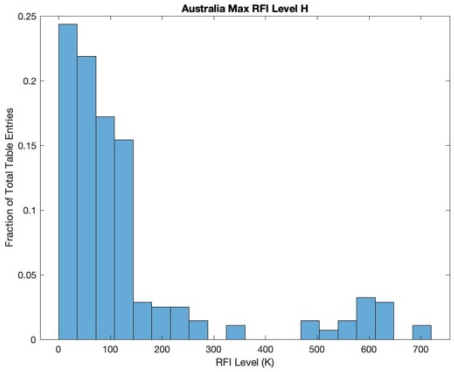
Australia Max RFI Level H
Fraction of Total Table Entries
RFI Level (K)

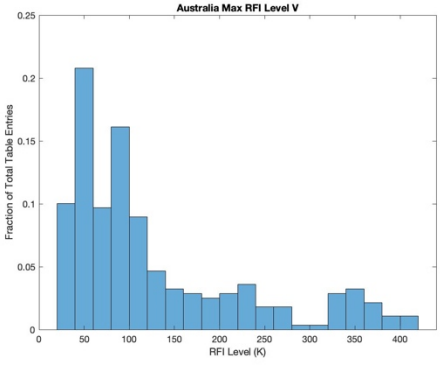
Australia Max RFI Level V
Fraction of Total Table Entries
RFI Level (K)

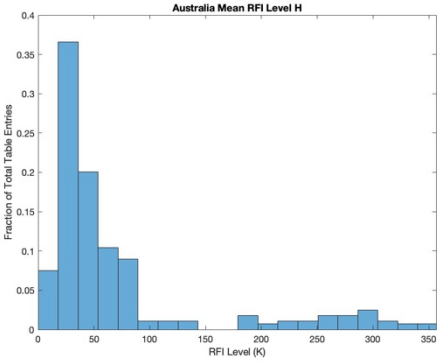
Australia Mean RFI Level H
Fraction of Total Table Entries
RFI Level (K)

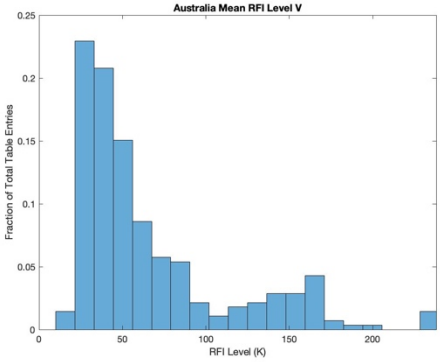
Australia Mean RFI Level V
Fraction of Total Table Entries
RFI Level (K)

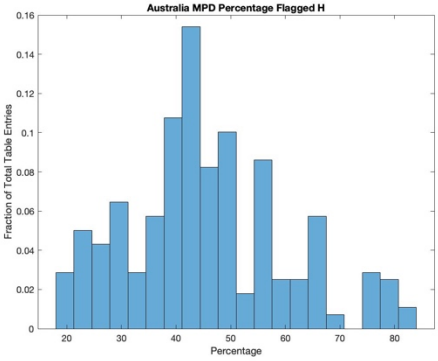
Australia MPD Percentage Flagged H
Fraction of Total Table Entries
Percentage

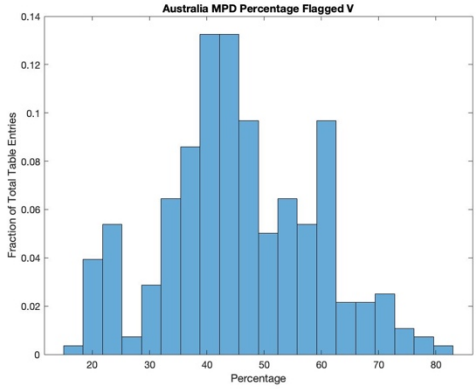
Australia MPD Percentage Flagged V
Fraction of Total Table Entries
Percentage

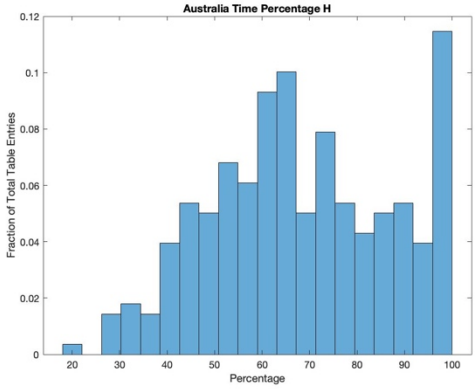
Australia Time Percentage H
Fraction of Total Table Entries
Percentage

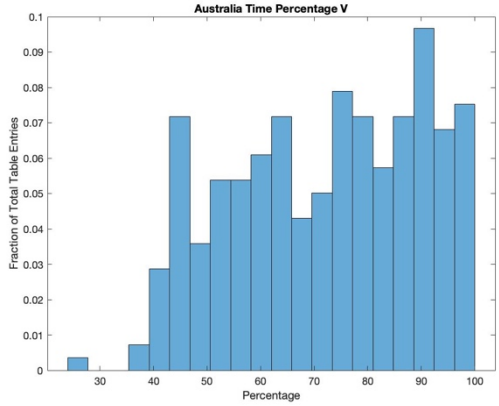
Australia Time Percentage V
Fraction of Total Table Entries
Percentage

Europe:

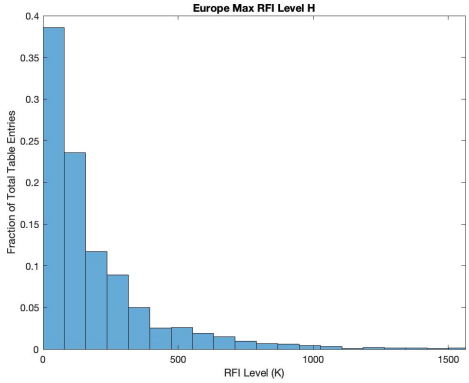
Europe Max RFI Level H
Fraction of Total Table Entries
RFI Level (K)

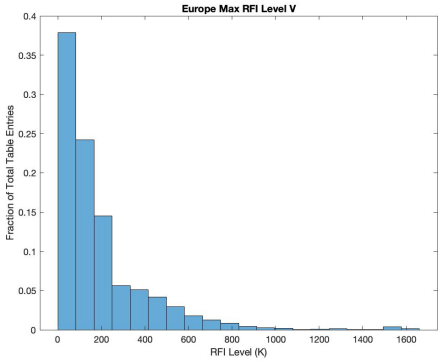
Europe Max RFI Level V
Fraction of Total Table Entries
RFI Level (K)

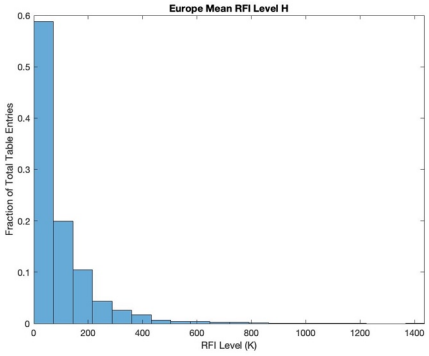
Europe Mean RFI Level H
Fraction of Total Table Entries
RFI Level (K)

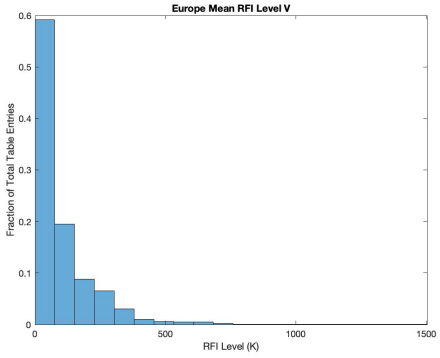
Europe Mean RFI Level V
Fraction of Total Table Entries
RFI Level (K)

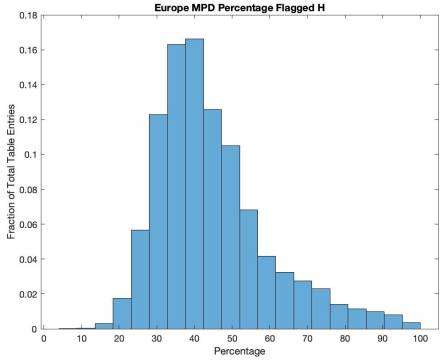
Europe MPD Percentage Flagged H
Fraction of Total Table Entries
Percentage

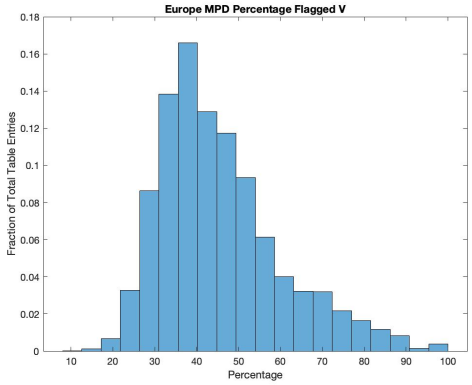
Europe MPD Percentage Flagged V
Fraction of Total Table Entries
Percentage

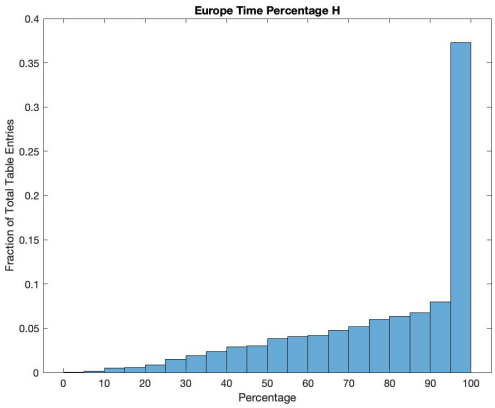
Europe Time Percentage H
Fraction of Total Table Entries
Percentage

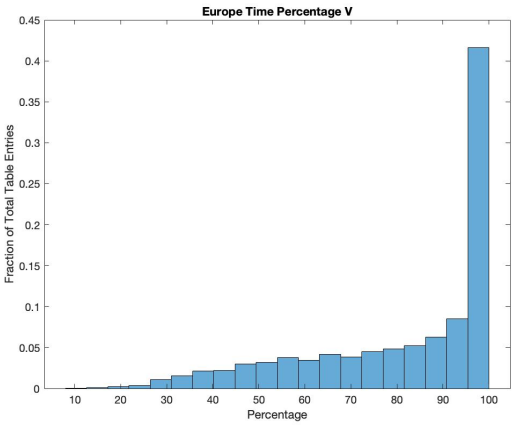
Europe Time Percentage V
Fraction of Total Table Entries
Percentage

North America:

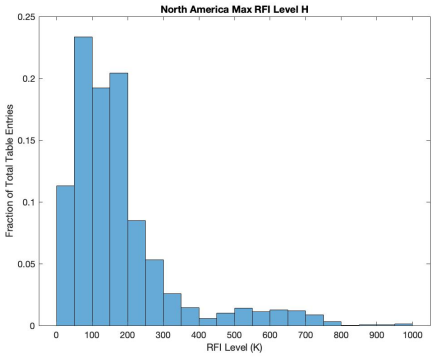

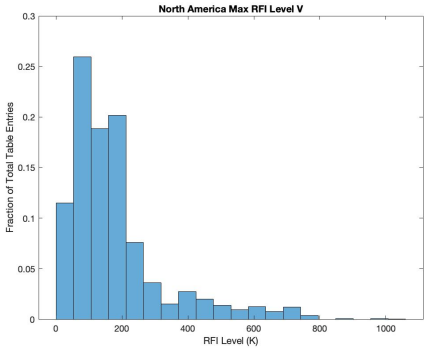

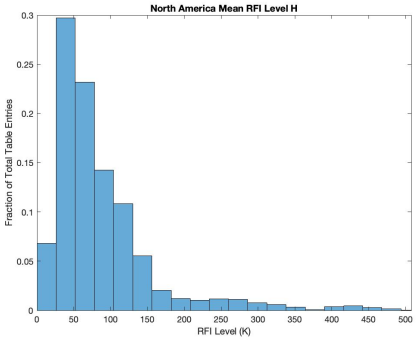

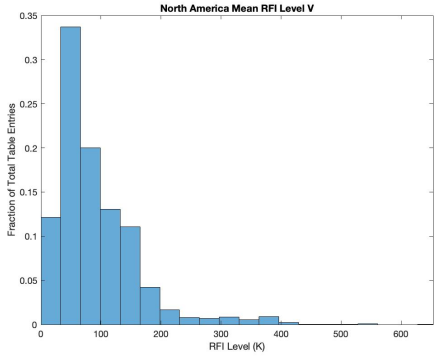

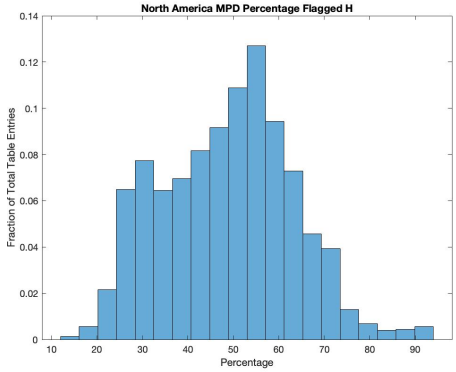

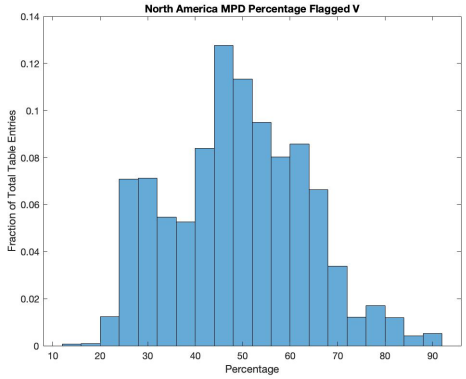

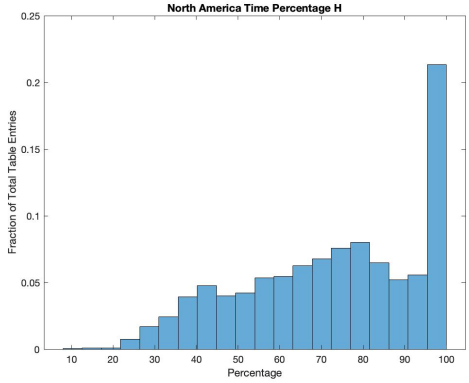

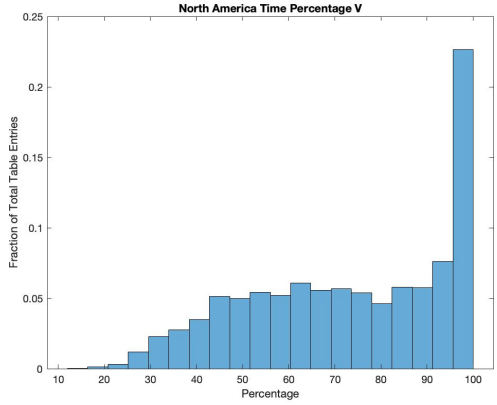

South America:

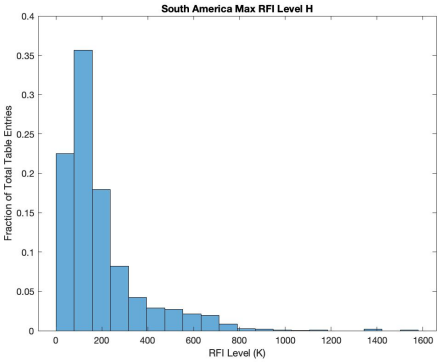

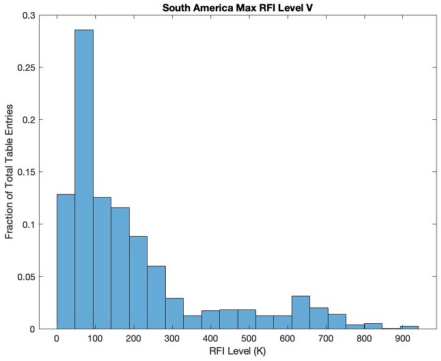

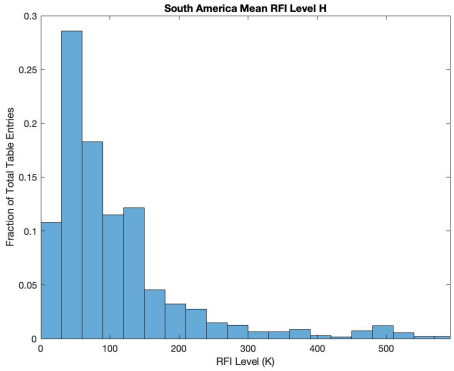

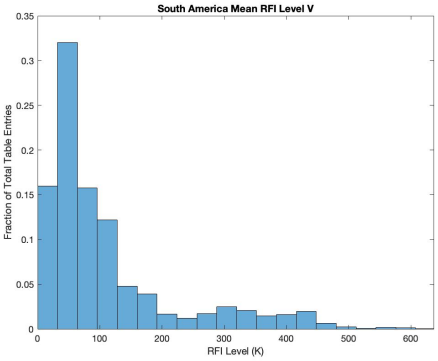

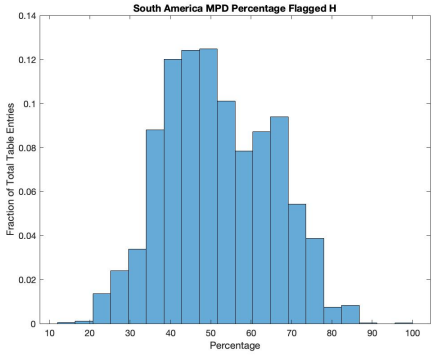

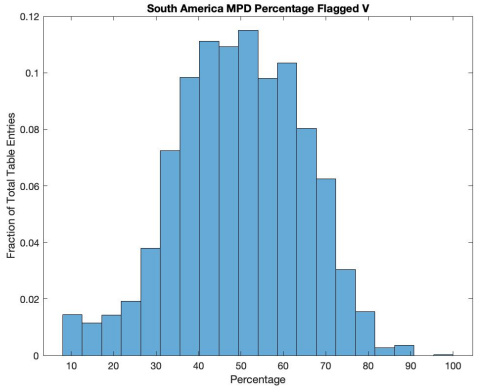

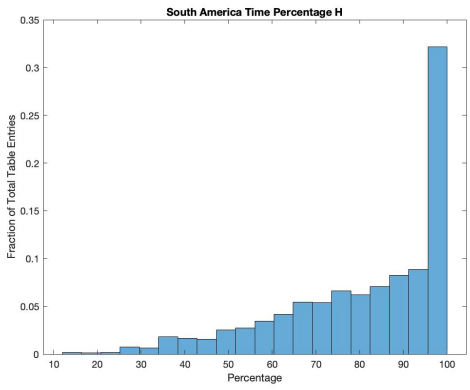

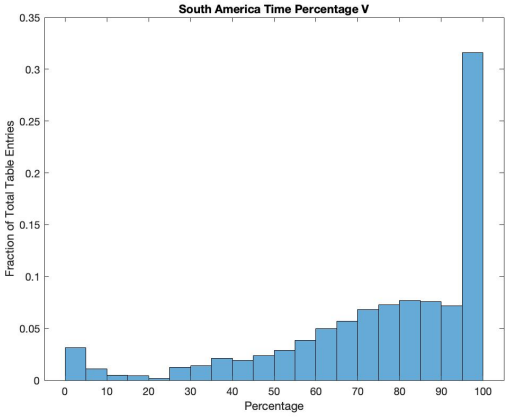

REFERENCES

[1] D. Entekhabi, et al, “The Soil Moisture Active Passive (SMAP) mission,” Proc. IEEE, vol. 98, no. 5, pp. 704–716, May 2010.

[2] J. R. Piepmeier, J. T. Johnson, P. N. Mohammed, D. Bradley, C. Ruf, M. Aksoy, R. Garcia, D. Hudson, L. Miles, and M. Wong, “Radio-Frequency Interference Mitigation for the Soil Moisture Active Passive Microwave Radiometer,” IEEE Trans. Geosci. Remote Sens., vol. 42, no. 1, pp. 761-775, Jan. 2014.

[3] J. T. Johnson, P. N. Mohammed, J. R. Piepmeier, A. Bringer and M. Aksoy, "Soil Moisture Active Passive (SMAP) microwave radiometer radio-frequency interference (RFI) mitigation: Algorithm updates and performance assessment," 2016 IEEE International Geoscience and Remote Sensing Symposium (IGARSS), Beijing, 2016, pp. 123-124.

[4] A. Bringer, M. Daehn, J. T. Johnson, Y. Soldo, D. M. Le Vine, P. de Matthaeis, J. R. Piepmeier, and P. Mohammed, “SMAP Mission: Changes in the RFI Environment,” IEEE International Geoscience and Remote Sensing Symposium, p. 3754-3757, July 2018.

[5] A. Bringer, M. Daehn, G. Weiss, and J. T. Johnson, “A Time Series Method for Identifying and Removing Residual RFI from SMAP L-Band Radiometer Data”, RFI Workshop, September 2019.

[6] A. Bringer, M. Daehn, G. Weiss, and J. T. Johnson, “New Methodologies to Identify and Remove Radio Frequency Interference (RFI): Demonstration with Data from the Soil Moil Active and Passive (SMAP) Mission”, CERF Technical Meeting, August 2019.

[7] P. Mohammed, M. Aksoy, J. R. Piepmeier, J. T. Johnson, and A. Bringer, “SMAP L-Band Microwave Radiometer: RFI Mitigation Prelaunch Analysis and First Year On-Orbit Observations”, IEEE Transactions on Geoscience and Remote Sensing 54.10 (2016): 6035-6047.